AN INVESTIGATION OF MORPHOLOGY OF POLYMERIC MICELLAR STRUCTURES IN THE PRESENCE OF PROTEIN FOR DRUG DELIVERY PURPOSES

A Thesis Submitted to
the Graduate School of Engineering and Sciences of
İzmir Institute of Technology
in Partial Fulfillment of the Requirements for the Degree of

MASTER of SCIENCE

in Chemistry

by
Gülistan KUTLUAY

July 2016
İZMİR

We approve the thesis of **Gülistan KUTLUAY**

Examining Committee Members:

_____

Prof. Dr. Hürriyet POLAT

Department of Chemistry, İzmir Institute of Technology

_____

Assoc. Prof. Dr. Gülşah Şanlı

Department of Chemistry, İzmir Institute of Technology

_____

Assist. Prof Dr. İlker POLATOĞLU

Department of Bioengineering, Celal Bayar University

28 July 2016

_____

Prof. Dr. Hürriyet POLAT

Supervisor, Department of Chemistry

İzmir Institute of Technology

_____

Prof. Dr. Ahmet E. EROĞLU

Head of the Department of Chemistry

_____

Prof. Dr. Bilge KARAÇALI

Dean of the Graduate School of Engineering and Sciences

ACKNOWLEDGEMENT

I would like to thank my thesis supervisor Prof. Dr. Hürriyet POLAT of the Science Faculty at İzmir Institute of Technology for her guidance, understanding, motivations and endless support during this study and preparation of this thesis.

I am grateful to Specialist Mine BAHÇECİ at İzmir Institute of Technology in the department of Center for Materials Research for her valuable help in AFM analysis.

I thank my family for their endless support, encouragement and help during this study.

Finally, I would like to thank to my husband, Harun AKTAŞ for his support, patience, encouragement, help and love.

This study supported by The Scientific and Technological Research Council of TURKEY (TÜBİTAK).

ABSTRACT

AN INVESTIGATION OF MORPHOLOGY OF POLYMERIC MICELLAR STRUCTURES IN THE PRESENCE OF PROTEIN FOR DRUG DELIVERY PURPOSES

Polymeric micellar structures are becoming increasingly important in drug delivery applications. Morphology of these structures is a factor determining the form and the amount of the drug to be enveloped as well as how the release mechanisms will function. Though there are numerous work on micelles in the literature in aqueous media, understanding is lacking with respect to the specifics of the micelle formation and the exact morphology of the micelles produced within simulated body fluids (SBF) that also contains protein. In this work, the well-defined micellar structures with and without bovine serum albumin (BSA) in SBF using some selected polymeric surface active agents (PEO-PPO-PEO tri-block copolymer, P-123) were studied.

The forms of P-123 molecules in distilled water (DW) and SBF (studied by surface tension measurements), micelle size distributions (studied by AFM, DLS, STEM, TEM), and electro kinetic potentials (studied by DLS) were the main parameters studied. DLS results showed that the average size of P-123 micelles did not change much in the presence of BSA in DW or SBF. In the cases of AFM, STEM and TEM, the sizes of P-123 micelles in the absence of BSA were comparable to the results of DLS. In the presence of BSA, on the other hand, the micelle structures come together to form large and loose aggregates in both DW and SBF.

When P-123 micelles loaded with drug, DLS results showed that the presence of drug in micelles does not change the size of micelles much in both water and SBF. But STEM results show a considerable increase in the sizes of P-123 micelles. The drug loaded micelles seem to aggregate in water and SBF in the absence of BSA and in water in the presence of BSA. But they seem to disperse in SBF in the presence of BSA.

ÖZET

İLAÇ TAŞIYICI AMAÇLI PROTEİN VARLIĞINDA POLİMERİK MİSEL YAPILARIN MORFOLOJİSİ ÜZERİNE BİR ARAŞTIRMA

Polimerik misel yapıların ilaç taşınımı konularında önemi giderek artmaktadır. Bu yapıların morfolojisi, ilaç salınım mekanizmalarında kullanılacak olan ilacın form ve miktarını belirleyecek faktördür. Sulu ortamda çalışılmış çok sayıda misel çalışmaları bulunmasına rağmen, yapay vücut sıvılarında protein varlığında misel oluşumu ve morfolojisi hakkındaki çalışmalar eksiktir. Bu çalışmada, iyi tanımlanmış olan misel yapılarının sığır serumu albumini (BSA) varlığında ve yokluğunda yapay vücut sıvısı içerisinde, seçilmiş olan bazı yüzey aktif maddeler ile çalışılmıştır.

P-123 molekülleri damıtılmış su ve yapay vücut sıvısı içerisinde ana parametreler olan yüzey gerilimi ölçümleri, misel boyut dağılımları (AFM, DLS, STEM ve TEM ile) ve elektro kinetik potansiyelleri (DLS ile) çalışılmıştır. DLS sonuçları, P-123 misellerinin ortalama büyüklüğünün damıtılmış su ve yapay vücut sıvısı içerisinde BSA varlığında çok değişiklik olmadığını göstermiştir. AFM, STEM ve TEM durumlarında, BSA yokluğunda P-123 misellerinin boyutları DLS sonuçları ile karşılaştırılabilir olmuştur. Diğer taraftan, misel yapıları BSA varlığında damıtılmış su ve yapay vücut sıvısı içerisinde büyük ve gevşek agregatlar oluşturmak için bir araya gelirler.

P-123 miselleri ilaç ile yüklü olduğunda, DLS sonuçları misellerin ilacın varlığında, su ve yapay vücut sıvısı içerisinde boyutunun çok değişmediğini göstermiştir. Ancak STEM sonuçları P-123 misel boyutlarında önemli bir artış olduğunu göstermiştir. İlaç yüklü miseller BSA yokluğunda su içinde ve yapay vücut sıvısı içerisinde, ve BSA varlığında su içerisinde agrega gibi görünmektedirler. Ancak BSA varlığında yapay vücut sıvısı içerisinde miseller dağılmış olarak görünmektedirler.

TABLE OF CONTENTS

LIST OF FIGURES

LIST OF TABLES

Table **Page**

CHAPTER 1

INTRODUCTION

1.1. Statement of the Problem

Controlled drug delivery system can be defined as a formulation which provides the delivery of drugs to specific targets of the body at a controlled rate. In these systems nontoxic and biocompatible material is used to load the drug and release it at a pre-determined rate while keeping the drug concentration in the therapeutic region. By use of these systems, the therapeutic drug level can be maintained for a prolonged period of time. Therefore, an ideal drug carrier should be inert, biocompatible, mechanically strong, capable of loading high amount of drug and releasing at a controlled rate and simple to administer and remove. Some of these carriers are, polymeric micelles, vesicles, nanospheres, liposomes, liquid crystals, nanocapsules, lipoproteins, microcapsules, and microparticles.

1.2. Polymeric Micelles as Commonly Used Drug Carriers

The delivery of therapeutic compounds can be hindered by their poor water solubility. Therefore, use of micellar structures for solubilizing these compounds has become extermely important. Micelles of tri-block copolymers is a promising example due to their unique structural composition; characterized by a hydrophobic core, which solubilizes the drug, and a hydrophilic corona which acts as a stabilizer (Jones et al., 1999; Gaucher, et al**.,** 2005; Sachs-Barrable et al., 2007; Plapied, et al., 2011; Hunter et al., 2012; Ensign, et al., 2012). Addition to this, polymeric micelles have many advantages than other carriers. For example, they are stable and can solubilize hydrophobic compounds in their inner core. Thus, polymeric micelles show very small cytotoxicity (Mourya et al., 2010). They have generally small size and their size can be easily controlled. Due to their hydrophilic shell and small size, they show long period of circulation in vivo and they can accumulate in tumoral tissues (Jones et al., 1999). Addition to this, hydrophilic shell of polymeric micelles interact with the plasma

proteins and cell membranes. Also, polymeric micelles naturally controls the biodistribution (Mourya et al., 2010).

Therefore polymeric micelles are potential carriers for the targeting of water insoluble drugs. However, the smaller polymeric micelles are effective for tissue accumulation/penetration in hypovascular tumor tissues (Mourya et al., 2010). Controlling of the size of polymeric micelles affects their length of time in the blood stream and efficiency of tumor tissue accumulation and penetration (due to their hydrophilic shell that interact with the plasma proteins and cell membranes) (Jones et al., 1999). They have been widely used for the delivery of anticancer drugs in preclinical and clinical studies (Kedar et al., 2010). However, these systems lack the well-control of the release of the entrapped molecules (Torchilin 2007).

The success rates with the drug-carriers are low than desired due to the difficulties encountered in the effective transport and controlled release in the target organs. The main reason for this is the natural barriers the drug must overcome during the transfer of the drug; i.e. the interaction of the carrier with the other components of the blood plasma. For example, the serum albumin which can easily bind to other compounds in the blood has a plasma concentration between 35 to 50 grams per liter. Therefore, an interaction between the serum albumin and the micellar structures is quite likely, affecting their physical and chemical structures, hence, the drug holding, organ targeting and controlled release abilities. Most data with respect to the use of polymeric surfactants in drug delivery is based on the work carried out in distilled water. However, presence of electrolytes and protein in solution should affect both the size and the shape of the surfactant molecules (due to the screening effect of the ionic species for example).

In literature, most of the studies are on protein-protein interaction. In some studies, AFM has been used to measure the energy of these interactions (Yaneva et al., 1997; Micic et al., 1999; Jiang et al., 2003; Wang et al., 2006; Xu, 2006; Ando, 2006; Ivanov et al., 2011; Elsayed, 2011). Some other studies are on the protein-simple surfactant interaction and complex formation. For example Kevin et al., 1998 studied the adsorption of BSA on PDADMAC (poly-diallyldimethylammonium chloride), PAMPS (poly-acrylamidomethylpropyl sulfonate), PMAPTAC (poly-methacrylamidopropyl trimethylammonium chloride), and PAMPS80AAm20' (AMPS-acrylamide copolimer) using light scattering and pH titration. Similarly Valstar et al., 2000 studied the BSA-surfactant interactions in aqueous solutions using fluorescence

probe and dynamic light scattering. Some researchers used surface tension measurements and SAXS (Santos et al., 2003) to study these type of interactions. Tribout et al., 1991 studied the interaction of Triton X-100 and BSA using surface tension measurements. Kiss et al., 2008 studied the interactions of surface that is modified with PEO/PPO/PEO block copolymer and poly lactic acid mixture, with BSA using Langmuir Baladged. AFM has been used to determine the surface roughness in this study. Opanasopit et al., 2005 studied the stability of drug-loaded micelles in the presence of BSA using high performance liquid chromatography (HPLC) and gel permeation chromatography (GPC) and found that BSA increases the stability of micelles. Mesa, 2005 studied the polymer-surfactant, protein-surfactant interactions and determine phase diagrams. In their study, permeability, viscosity measurements and TEM, AFM, NMR, fluorescence spectroscopy were used. Shweitzer et al., 2004 studied the change in the size of a simple surfactant micelle (Sodium dodecyl sulfate) in the presence of BSA using surface tension measurements, fluorescence spectroscopy and SAXS.

As a conclusion, there are basic studies which focus on the compatability and interactions between various chemotherapeutic agents such as doxorubicin and surfactants, between surfactants and proteins and between various proteins. However, there are no detailed study on the effect of these interactions on the morphology and physicochemical structure of the polymeric micelles. A systematic in depth-investigation of these factors with advanced in-situ methods is extremely important in designing smart drug delivery carriers and constitutes the topic of this study.

1.3. Scope of the Study

In this thesis, we proposed to investigate the morphology of polymeric micelle structures in the presence of Bovine Serum Albumin (BSA) for drug delivery purposes. For this purpose, the most commonly used block co-polymer, P-123 (with 40% hydrophilicty) was used as polymeric surfactant to form micelles as drug carrierss. The physical and chemical properties of the micelles were characterized by DLS (for micelle size distribution and surface charge), AFM (for micelle size distribution, topography measurements,), TEM and STEM (for micelle size distribution, micelle shape, topography measurements). The results are presented and discussed to evaluate together in the following paragraphs.

CHAPTER-2

GENERAL INFORMATION

2.1. Polymeric Surfactants

Simple Surface Active Agents (SURFACTANTS) are chemicals that adsorb at surfaces/interfaces due to their dual property structure. They lower the surface tension of the liquid. They can use in many applications, for example foaming, detergency, emulsification, lubrication, dispersion stabilization, and formulation of cosmetics and inks, etc. Surfactants are amphiphilic molecules. As seen in Figure 2.1., they include hydrophilic and hydrophobic part in one molecule. Hence, surfactant molecule contains water soluble and water insoluble component.

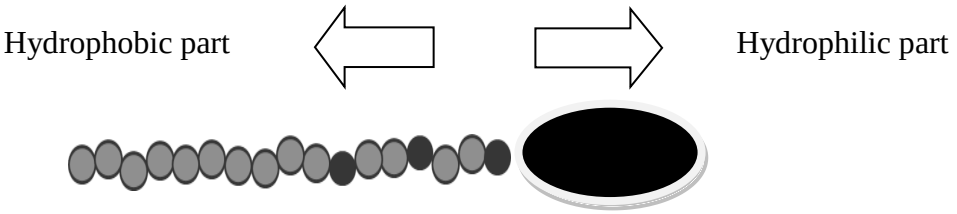

Figure 2.1. Surfactant molecule.

Hydrophilic part is headgroup and a hydrophobic part is tail. The headgroup of surfactants can be anionic, cationic, nonionic and zwitterionic. Tail part of surfactants consist of hydrocarbon chains.

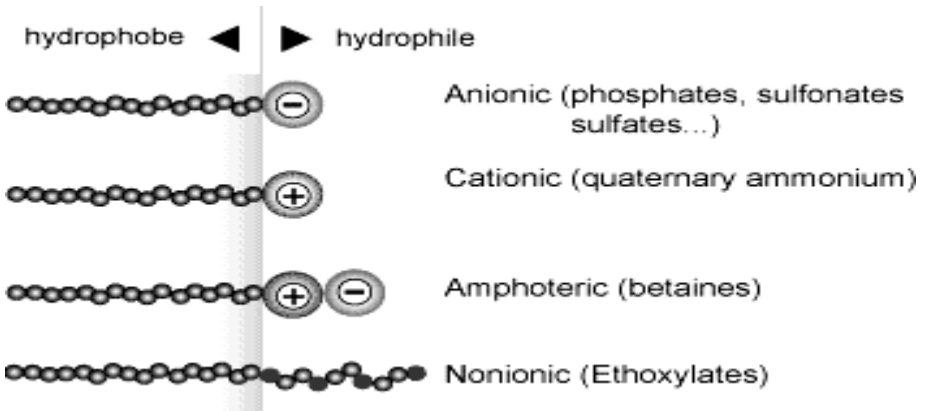

Figure 2.2. Types of surfactants.

Surfactants have types as seen in Figure 2.2. Addition to these types, surfactants have polymeric surfactant type.

1) ANIONIC SURFACTANTS
2) NONIONIC SURFACTANTS
3) CATIONIC SURFACTANTS
4) AMPOTHERIC SURFACTANTS
5) POLYMERIC SURFACTANTS

a) Random Copolymer
b) Diblock Copolymer
c) Tri-block Copolymer
d) Graft Copolymer
e) Star Copolymer

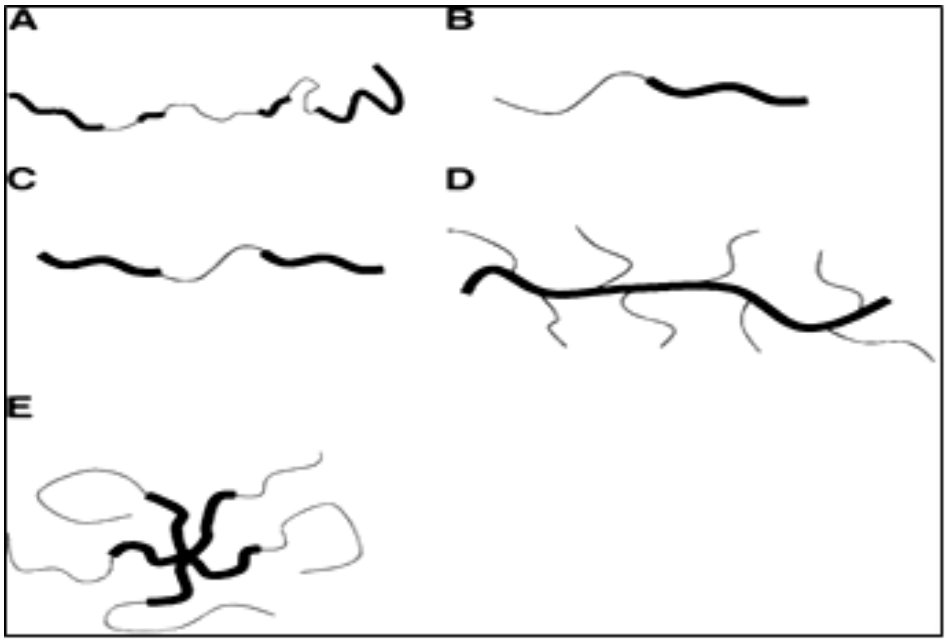

Figure 2.3. Different copolymer architectures: (A) random copolymer, (B) diblock copolymer, (C) tri-block copolymer, (D) graft copolymer, and (E) star copolymer.

Copolymers are synthesized by the simultaneous polymerization of more than one type of monomer. If the individual monomers occur various lengths of blocks in the copolymer molecule, result synthesis is called as block copolymer.

In this thesis, we used tri-block copolymer to obtain micelles as drug carriers. Tri-block copolymers poly (ethylene oxide) – poly (propylene oxide) – poly (ethylene oxide),

often denoted as PEO-PPO-PEO or $(EO)_a(PO)_b(EO)_a$. Variation of PPO/PEO ratio and lengths of PEO and PPO blocks during synthesis leads to the production of molecules with specific requirements in various areas of technological significance. Commercial names for Tri-block copolymers are Poloxamers, Synperonics (manufactured by ICI) and Pluronics (manufactured by BASF).

P-123 was used as the tri-block copolymer in this thesis. It has **s**tructural composition is $HO(C_2H_4O)_{20}(C_3H_6O)_{70}(C_2H_4O)_{20}H$. Its average molecular weight is 5800 g/mol. The $PEO_{20}PPO_{70}PEO_{20}$ micelles are amphiphilic and they consist of a hydrophilic PEO shell and a hydrophobic PPO core. Pluronic P-123 is a difunctional block copolymer surfactant terminating in primary hydroxyl groups. A nonionic surfactant that is 100% active and relatively nontoxic.

Table 2.1. The chemical formula and molecular weight of the Pluronic P-123.

Commercial name	Chemical formula	Molecular weight (g/mol)
Pluronic P-123	$PEO_{20}PPO_{70}PEO_{20}$	5800

Table 2.2. Properties of the Pluronic P-123.

A	B	C	D	E	F	G	H	I
P-123	5750	30	31	350	34	45	90	7-12

A: copolymer B: average molecular weight C: PEO wt.% D: melting pour point ('~C) E: viscosity (Brookfield) (cps;liquids at 25~C, pastes at 60'~C, solids at 77:C) F: surface tension at 0.1%, 25'~C (dyn cm ~) G: foam height (mm)(Ross Miles, 0.1% at 50:C) H: cloud point in aqueous 1% solution (:C) l: HLB (hydrophilic-lipophilic balance).

2.2. Polymeric Micelles

Polymeric micelles are created by a spontaneous self-assembly of polymeric molecules. These molecules are synthetic amphiphilic di-block or tri-block copolymers. They include hydrophilic and hydrophobic blocks. Generally, micelles have spherical shape. It contains a hydrophobic core and hydrophilic corona. Spherical micelles' hydrodynamic diameter ranges from 20nm to 80nm (Petrov et al., 2008). Micelles have more arrangements. These arrangements are, spherical, cylinder or rod, hexagonal, and

lamellar micelles as seen in Figure 2.4.. Higher concentrations and temperatures, increase in aggregation number, addition of salts, cosolvents and surfactants change the critical micelle concentration and shape of micelles.

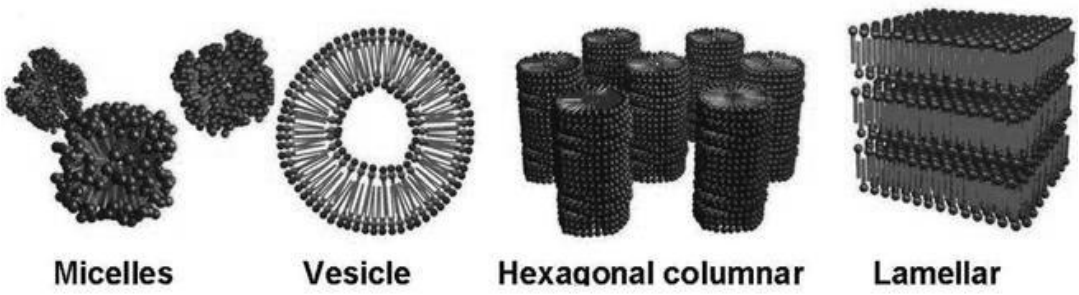

Figure 2.4. Shapes of micelles.

According to solvent is used to obtaine polymeric micelles, micelles can be formed direct micelle as seen in Figure 2.5. or reverse micelle as seen in Figure 2.6..

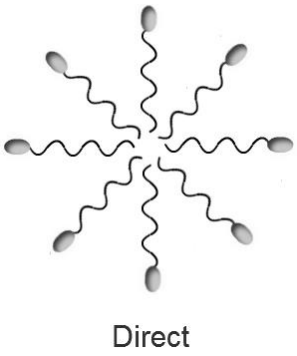

Figure 2.5. Representation of direct micelle.

In a micelle, hydrophilic part form an outer shell in contact with water and hyrophobic part forms the core of a micelle.

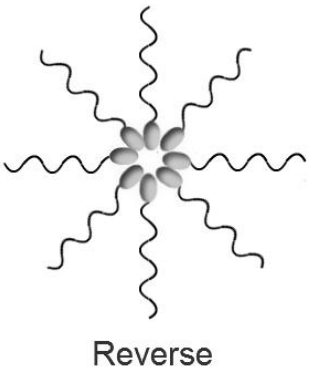

Figure 2.6. Representation of reverse micelle.

In a reverse micelle, hyrophobic part form an outer shell in contact with water and hydrophilic part forms the core of a micelle in low polar solvents.

The critical micelle concentration (CMC) is the copolymer concentration at which micelles start forming. At low concentrations, copolymer molecules are formed in unimers. Copolymer molecules' self-assembly starts when the concentration reaches specific value and micelles are formed. The CMC is directly related with length of a hydrophobic part. If the length of a hydrophobic part is long, CMC is lower. For Pluronic family, CMC is in the range of 10^{-4}-10^{-3} M and this value is highly dependent on the hydrophilic-hydrophobic ratio in the copolymer molecule (Rapoport, 2007).

2.3. Protein Structures and Bovine Serum Albumin

Proteins are built up by amino acids that are linked by peptide bonds into a polypeptide chain. Simple proteins are polymers formed by condensation of amino acids. The condensation reaction occurs between the amino group of one amino acid and the carboxyl group of another, forming peptide bond by the following reaction:

$H_2N.CHR_1.COOH + H_2N.CHR_2.COOH$ ------$H_2N.CHR_1.CONH.CHR_2.COOH + H_2O$

All the amino acids have a central carbon atom (Cα) to which a hydrogen atom, an amino group (NH_2), a carboxyl group (COOH) and a residue group (R) are attached. There

are 20 different R groups. Amino acids contain two or more polar functional groups such as –NH, -OH, -COOH, and –SH. Therefore they are chemically reactive and subjected to chemical attack. Hence proteins are unstable. These groups give protein polyelectrolyte character (Franks, 1993). Its charge depends on pH of the medium.

Protein structure can be described regarding with four levels. First level is primary structure. This is array of amino acids in protein structure. Second level is the secondary structure. This level refers to spatial array of polypeptide chains. The secondary structure elements bend into structural units. These structures called as domains and they include the tertiary structure. Third level is tertiary structure. It has 3D structure of functional protein. Finally, fourth level is quaternary structure. Quaternary structure comprised array of two or more polypeptide chains.

Proteins can be classified as two groups according to their shape properties. These proteins are fibrous proteins and globular proteins.

1) FIBROUS PROTEINS

Fibrous proteins are not soluble in water and they have helical or sheet structure.

2) GLOBULAR PROTEINS

Globular proteins are soluble in water and they have spherical shape.

Proteins can be disrupted with high temperature, pH changes, surfactants, and chaotropic agents.

Bovine Serum Albumin (BSA) is constituted by the twenty essential amino acids within a structure that contains 583 units. Approximate molecular dimensions of BSA is 4 × 4 × 14 nm. BSA is very similar to the human serum albumin (HAS) and its structure and physicochemical properties are well characterized. BSA has negative charge hence it has high binding capacity and it is soluble in water. Also, BSA is used as a model protein for various biomedically related studies.

Table 2.3. Some important properties of Bovine Serum Albumin.

Molecular weight (g/mol)	Density (g/cm3)	Pzc (PI)	Dimensions (nm)
66.000	1.36	4.7-4.9	4x4x14

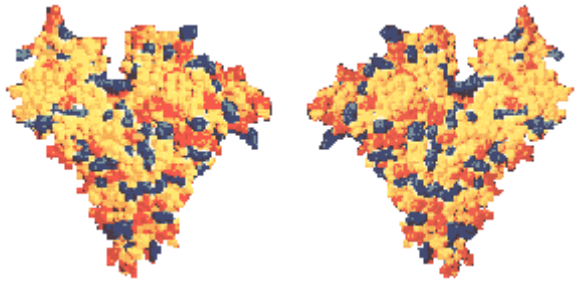

A B

Figure 2.7. Space filling model of serum albumin molecule with basic residues coloured in blue, acidic residues in red, and neutral ones in yellow (A) Front view, (B) back view(Carter and Ho, 1994).

Addition to these, BSA has three principal domains. These domains change with different pH values. For example, between pH 5 - pH 8, BSA has N form ‘N (normal)’, between pH 3 - pH 4, BSA has F form ‘F (fast)’, and if pH < 3, BSA has E form ‘E (expanded)’ (Jachimska et al., 2012).

In this thesis, BSA protein was used because it has many advantages. For example, it is derived from cows, its cost is low, it does not effect other enzymes, it is nutrient for cell and microbial cultures, and it is widely used for biochemical applications.

2.4. Polymeric Micelles as Drug Carriers

Polymeric micelles have core and corona part. Core part is formed by hydrophobic block of copolymer and corona part is formed by hydrophilic block of copolymer. Polymeric micelles have many advantages for drug carrier. First of all, they are stable towards dilution also show minimal cytotoxicity. They have small sizes and can solubilize hydrophobic drugs in their inner core, non-toxic, used for induce immune responses, inhibiting P-glycoprotein. Shell of polymeric micelles stabilizes the micelle, interacts with the plasma proteins and cell membranes and controls biodistribution of the carrier. Because of these reasons, they are used as a carrier for poorly water soluble drugs (Jones et al 1999, Mourya et al. 2010).

2.5. Other Commonly Used Drug Carriers

Drug delivery by the aid of nanoparticles has given rise to numerous studies and these have been reviewed in a detailed way (Kim et al., 2010; Yokoyama, 2005). These nanocarriers can be classified into several types such as nanospheres, nanocapsules, nanotubes, nanogels and dendrimers etc. The biological molecules are able to be delivered by the dissolution within a polymeric matrix, entrappment inside lipid, encapsulation or adsorption onto the surfaces of the particles (Mishra et al., 2010).

Polymeric nanoparticles are prepared from a synthetic polymeric block and can be used to deliver drug molecules. Depending on the preparation method, polymeric nanoparticles in which the drug is confined to a cavity surrounded by a polymeric membrane or nanospheres consisting of matrix systems in which the drug is dispersed can be obtained. Biodegradable polymers such as polylactic acid (PLA), poly (glycolic acid) (PGA), poly (lactic-co-glycolic acid) (PLGA) are usually used in these applications due to the fact that these structures can be easily hydrolyzed into monomers which can be excreted from the body through metabolic pathways. Another advantage of using these nanoparticles is that it provides the sustained release of drugs within the target site over a specific period. However, the use of these nanoparticles (especially including non-biodegradable polymers) may have several disadvantages such as the cytotoxicity of by-products and scalability (Ochekpe et al., 2009).

Liposomes are small, spherical systems which are usually synthesized from cholesterol and nontoxic phospholipids. Due to being natural, their size, hydrophobic and hydrophilic character and biocompatibility, they have been one of the promising drug carriers. They can exhibit different properties affected from their size, shape, method of preparation and surface charge. Moreover, they can be present in several forms based on their size and number of layers: Small unilamellar vesicles, large unilamellar vesicles and multilamellar vesicles. They are considered reducing the toxicity and delivering the drugs within the body for a prolonged period. However, they may have low encapsulation efficiency and causes rapid leakage of the water soluble drug molecules in the blood stream (Sahoo et al., 2003).

Solid lipid nanoparticles are the colloidal structures composed of physiological lipid, dispersed in water or aqueous surfactant solution. As a drug carrier, they are usually made up of a solid hydrophobic core containing dissolved or dispersed drug. Although these structures provide site-specific targeting, high stability, controlled drug

release and good tolerability, they have insufficient drug loading and drug expulsion through storage. In order to overcome these limitations, liquid lipids with improved drug delivery characteristics may be incorporated (Ochekpe et al., 2009; Mishra et al., 2010).

Magnetic nanoparticles are also among the promising materials in biomedical applications such as drug delivery and imaging. The magnetic structure such as iron oxide or magnetite are present in the core of the particle which is coated by an inorganic or polymeric structure in order to make the particles biocompatible, stable and a support for drug molecules. The key features in the behaviour of these nanoparticles are based on their surface chemistry, size (magnetic core, size distribution) and magnetic properties. Their limitations are the relation between the drug delivery performance and the capacity of the external magnetic field, and the accumulation of the magnetic nanoparticles with respect to the geometry of the magnetic field (Arruebo et al., 2007).

Dendrimers are highly branced macromolecules consisting of an initiator core, interior layers attached radially to the core and possessing repeating units, and exterior part. In drug delivery applications, drugs can be encapsulated in the void spaces within the dendrimer structure and interaction of drug and dendrimer can be provided via electrostatic or covalent bonds at the terminal groups. The dendrimer structure can allow the surface functionalization, possess multivalency and ease of preparation. Both hydrophilic and hydrophobic drugs can be delivered by these nanostructures. However, these nanoparticles have several limitations related to their high cost, the challenge in the avoidance of long-term accumulation within the body and the toxicity depending on the density and nature of the charged groups at the terminal groups and their size (Arruebo et al., 2007)

Carbon based nanoparticles, especially nanotubes and porous structures, have shown promising behaviours in drug delivery applications. Carbon nanotubes are extremely small tubes which consists of either single or multi wall carbon structure. Their special structures make them good candidates to encapsulate drug molecules in their cavities. However, the toxicity of these nanocarriers has been of concern, especially when using without surface modifications. To reduce their toxicity in blood stream, the studies has been continued. In addition to the carbon nanotubes, porous carbon particles has been started to be used as drug carrier due to their good surface characteristics such as high surface area, adjustable pore sizes, and stability even in the harsh acidic stomach conditions (Xu et al., 2008).

Among the ceramic based materials, silica nanoparticles have been extensively studied in drug delivery applications. Especially mesoporous silica nanoparticles are used successfully as a drug carrier due to their high surface-to-volume ratio, well-controlled pore characteristics, inertness and biocompatibility. However, the toxicity of these nanoparticles may be concern when they are used at high dosages and exposure time (Jong et al., 2008).

CHAPTER-3

MATERIALS and METHODS

3.1. Materials

3.1.1. Polymeric Surfactant and Other Chemicals

In this study, $PEO_{20}/PPO_{70}/PEO_{20}$ type of tri-block copolymer, P-123 (SIGMA ALDRICH) was used to create micelles. The molecular weight of this surfactant was reported to be 5800 g/mol and its chemical formula is given in Table 3.1.

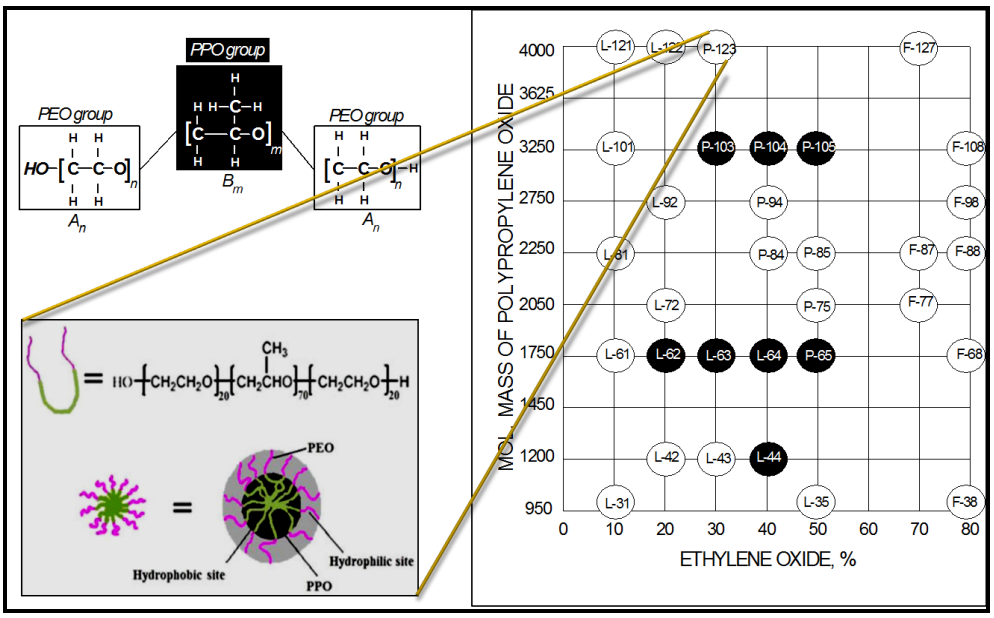

Figure 3.1. Molecular structure of pluronic tri-block-copolymers (A_n: # of ethylene oxide (EO) groups, B_m: # of propylene oxide (PO) groups.

Albumin from Bovine Serum (BSA) (SIGMA ALDRICH, 96%) was used as protein to refer human serum albumin (HAS). Methanol (SIGMA ALDRICH) was used for solvent and co-solvent evaporation methods to encapsulate drug in micelles.

3.1.2. Probucol as a Model Drug

Probucol was used as a model hydrophobic drug and obtained from SIGMA ALDRICH. The chemical structure of probucol is given in Figure 3.2 and table 3.1. Probucol is known to lower the level of cholesterol in the bloodstream and increase the rate of LDL catabolism. Therefore it is used to lower LDL (Low-density lipoprotein) and HDL (High-density lipoproteins) cholesterol.

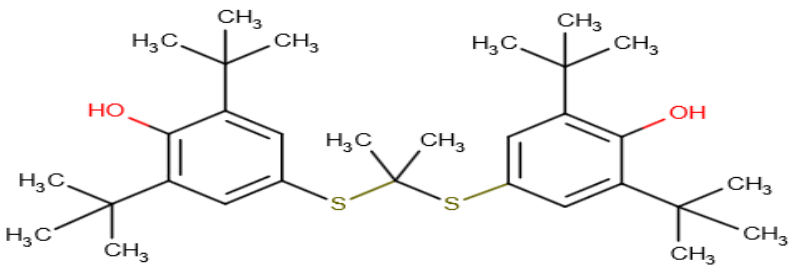

Figure 3.2. Probucol Structure.

Table 3.1. Probucol drug properties.

Chemical Formula	$C_{31}H_{48}O_2S_2$
Protein binding	Not Available
State	Solid
Melting Point	125 °C
Water Solubility	4.18e-05 mg/mL

3.1.3. Mica Surface

General structure of mica is 'AB_{2-3}(Al, Si)Si_3O_{10}(F,OH_2)' where, A can be potassium (K), calcium (Ca), sodium (Na), or barium (Ba) and sometimes other elements, B can be aluminum (Al), lithium (Li), iron (Fe), or magnesium (Mg) elements. Mica materials are composed of six forms found in nature. These forms are muscovite, biotite, phlogopite, lepidolite, fuchsite, and zinnwaldite. Muscovite mica is the most plentiful type of mica and it is a suitable surface to form himemicelles (Rojas, 2002) (Table 3.2, Figure 3.3).

Table 3.2. Chemical composition of Mica V1.

Silica (SiO_2)	45.57%
Alumina (Al_2O_3)	33.10%
Potassium Oxide (K_2O)	9.87%
Ferric Oxide (Fe_2O_3)	2.48%
Sodium Oxide (Na_2O)	0.62%
Titanium Oxide (TiO_2)	Traces
Calcium Oxide (CaO)	0.21%
Magnesia (MgO)	0.38%
Moisture at 100^oC	0.25%
Phosphorus (P)	0.03%
Sulphur (S)	0.01%
Graphite Carbon (C)	0.44%
Loss on Ignition (H_2O)	2.74%

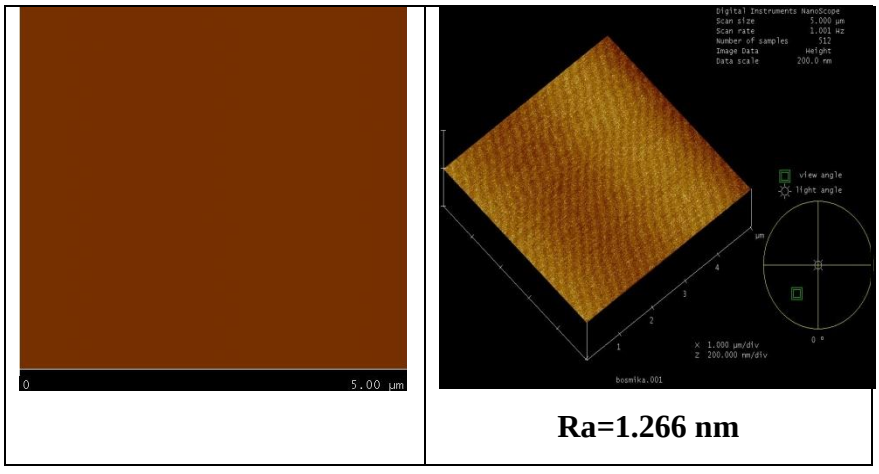

Ra=1.266 nm

Figure 3.3. AFM image of empty mica surface.

3.1.4. Copper Grid

200 square mesh copper grids support with carbon film were used for obtain TEM and STEM images of P-123 micelles with and without BSA protein in DW and in SBF. Addition to these, tem grids were used for drug encapsulation STEM images.

3.2. Experimental Methods

3.2.1. Preparation of Solutions and Formation of Hemi Micelles

10^{-2}M, 10^{-3}M, 10^{-4}M P-123 solutions that contain micelles were prepared both in distilled water (DW) and Simulated Body Fluid (SBF). The solutions were stirred overnight at room temperature. In some cases, BSA was also added to study the changes in the morphology of micelles.

Hemi micelles were obtained on the mica surfaces to study the morphologies of micelles by AFM, TEM and STEM. To obtain hemi micelles, the mica surfaces (after separating the top layers of mica surfaces) were immersed in tri-block copolymer micelle solution for 15 seconds. Then these surfaces were placed on glass surfaces and dried for 7 days at room temperature under 1 bar.

3.2.2. Preparation of Simulated Body Fluid (SBF)

Simulated body fluid was prepared by dissolving reagent grade chemicals of NaCl, $NaHCO_3$, KCl, K_2HPO_4, $MgCl_2.6H_2O$, $CaCl_2.2H_2O$ and Na_2SO_4 in deionized water. They were added to the solution in the order to list given below (Table 3.3). The solution was buffered at physiological pH 7.4 at 37^oC with 50 mM trishydroxymethyl aminomethane [$(CH_2OH)_3CNH_2$] (THAM) and 36.23 mM HCl acid. Then this solution was compared with human plasma (Table 3.4).

Table 3.3. Composition of the SBF.

Order	Reagents	Amounts
1	NaCl	7.996 g
2	$NaHCO_3$	0.350 g
3	KCl	0.224 g
4	$K_2HPO_4.3H_20$	0.228 g
5	$MgCl_26H_2O$	0.305 g
6	1M-HCl	40 ml
7	$CaCl_2$	0.278 g
8	Na_2SO_4	0.071 g
9	$(CH_2OH)_3\ CNH_2$	6.57 g

Table 3.4. Composition of SBF and human blood plasma (Source: Olivera et al., 1995).

	Plasma (mM)	SBF (mM)
Na^+	142.0	142.0
K^+	5.0	5.0
Ca^+	2.5	2.5
Mg^+	1.5	1.5
Cl^-	103.0	148.0
HCO^-_3	27.0	4.2
HPO^{2-}_4	1.0	1.0
SO^{2-}_4	0.5	0.5

3.2.3. Loading Drug into Micelles

3.2.3.1. Solvent Evaporation Method

To make drug loading into the micelles, once a suitable polymer has been identified, and then the drug must be loaded into the micelles.

In solvent evaporation technique, a volatile organic solvent is used to dissolve copolymer and drug at the same time. Volatile organic solvent is evaporated under

vacuum and thin film of copolymer and drug is obtained. After this step, distilled water and simulated body fluid are added to copolymer and drug film separately and drug-loaded polymeric micelles are obtained.

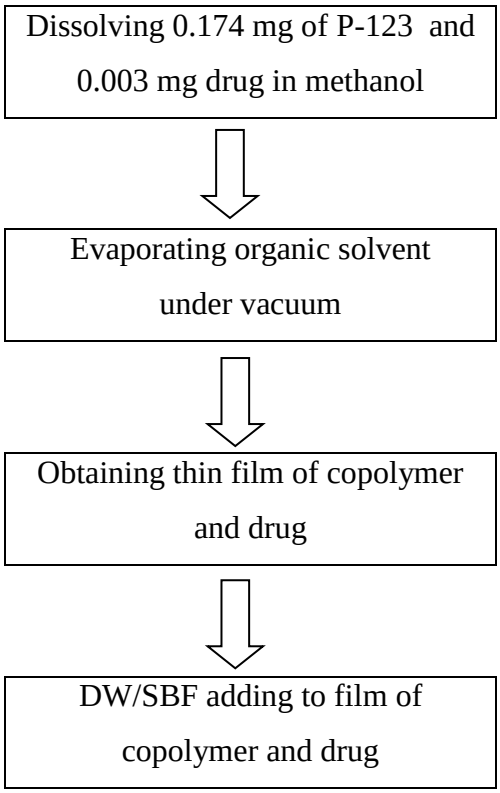

Figure 3.4 Solvent evaporation method for drug encapsulation in micelles in DW and SBF.

3.2.3.2. Co-Solvent Evaporation Method

To make the self-assembly of the micelle and encapsulation of the drug into the micelles, co-solvent evaporation method can be used. In co-solvent evaporation technique, copolymer, drug, volatile organic solvent, and water or SBF are solved at the same time. Volatile organic solvent is evaporated under vacuum drug-loaded polymeric micelles are obtained.

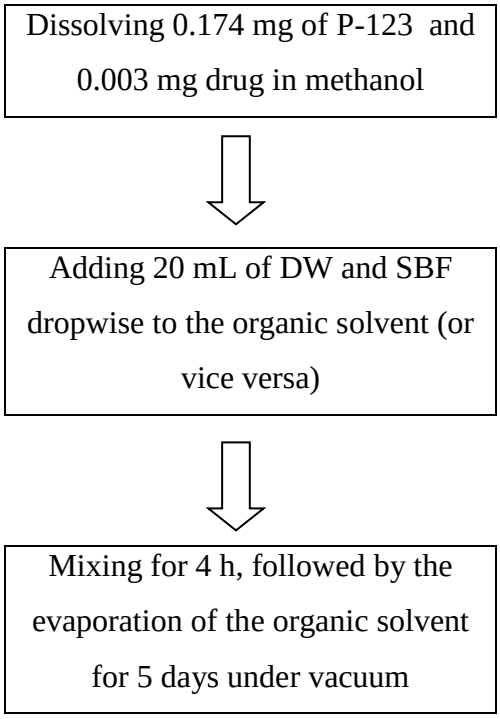

Figure 3.5. Co-Solvent evaporation method for drug encapsulation in micelles in DW and SBF.

3.2.4. Surface Tension Measurements

Surface tension measurements were conducted with P-123 at different concentrations of 10^{-2}, 10^{-3}, 10^{-4}, 10^{-5}, 10^{-6}, 10^{-7} M. For surface tension measurements, Kruss Model Digital Tensiometer (K10ST) with the Du-Noüy Ring method was used (Figure 3.6). The ring is usually made up of platinum or platinum-iridium alloy. Radius (R) of this ring is 2-3 cm. The measuring device is a vertically suspended ring with a precise geometry. When the ring is brought into contact with the liquid, the liquid "jumps" to the ring and pulls it into the liquid. The force caused by this wetting is measured by pulling the ring up to the level of the liquid surface (Adamson, 1997). The surface tension of the liquid is determined from the measured force using the equation (3.1):

$$\Upsilon = F/pCosQf \qquad (3.1)$$

where ϒ is the surface tension, F is the maximum force, p is the perimeter of the three-phase contact line (p = 4pR) and f is a correction factor due to additional volume of liquid is lifted during the detachment of the ring from the interface and is contact angle measured for the liquid meniscus in contact with the ring surface (Drelich et al., 2002).

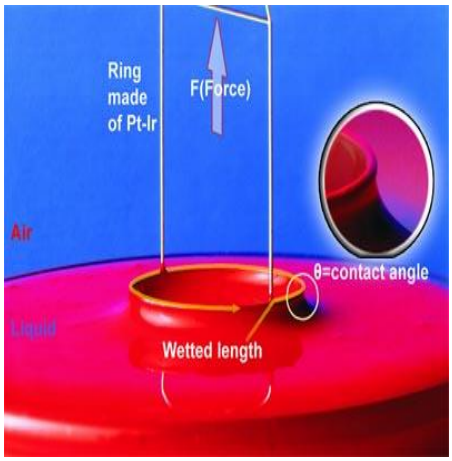

Figure 3.6. A Kruss model digital tensiometer (K10ST) used for surface tension measurements.

3.2.5. Size and Charge Measurements

Zeta potential measurements were applied to P-123 solutions to observe micelles in DW and SBF with and without BSA. Size and zeta potential measurements of micelles were carried out using Malvern Zeta Sizer Nano ZS. The device employs a combination of laser Doppler velocimetry and Phase Analysis Light Scattering (PALS).

Malvern Zeta Sizer uses dynamic light scattering method and working principle based on the fact that spatial distribution of scattered light is a function of the particle size of the analyzed sample. Size of particles which are measured by the method is inversely proportional to angle seen after the particles scatter light. In other words, small particles scatter light at small angles while large particles scatter light at small angles relative to the laser beam. These particles pass through a focused laser beam during the laser diffraction measurement. A series of photosensitive detectors are used to get the angular intensity of scattered light. Particle size is calculated by using the map of scattering intensity versus angle. Particles are moving because of Brownian motion

which is due to random collision with the molecules of the liquid that surrounds the particle. Stokes-Einstein equation defines the relationship between size of particle and its speed due to Brownian motion and Zeta Sizer uses the relationship to obtain size. There are some specialties to prefer Laser diffraction technique such as wide dynamic range, repeatability, rapid measurements, instant feedback, high sample throughput, no need to calibration.

Surface charge of nanoparticles or the potential that is at particle surface is called as Zeta potential. Malvern Zeta Sizer Nano ZS (Figure 3.7) is used to obtain zeta potential by using Henry equation. Henry equation is (3.2):

$$UE=(2\varepsilon z f(ka))/3\eta \qquad (3.2)$$

where z is the zeta potential, UE is the electrophoretic mobility, Ɛ is the dielectric constant, Ŋ is the viscosity, f(ka) is the Henrys function, and f (ka) value generally used as 1.5 or 1.0.

Potential stability of the colloidal systems can be understood by the magnitude of the zeta potential. In colloidal systems, if the particles have low zeta potential values, particles can come together and flocculate. On the other hand, if all the particles have a large negative or positive zeta potential values, they will repel each other and they can not flocculate.

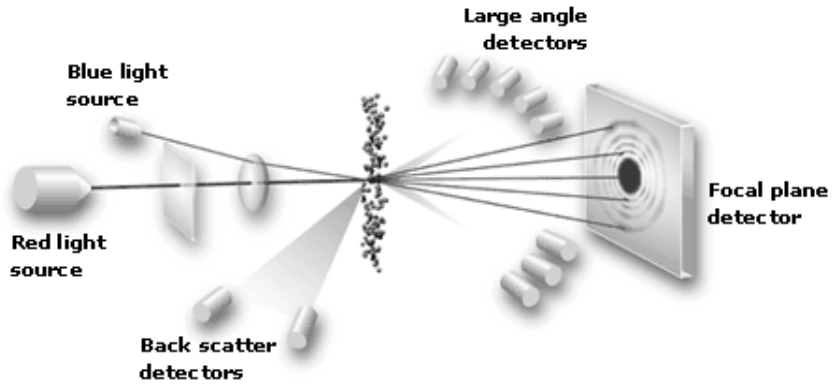

Figure 3.7. Malvern Mastersizer 2000 Laser Diffraction.

3.2.6. STEM Analysis

STEM characterizations were performed by using a Quanta 250FEG type instrument. In STEM analysis, the reflected electron beam is limited by a raster across the surface of the sample and the image is obtained by counting backscattered electrons.

Before the STEM analysis, P-123 surfactant micelles were obtained in DW and SBF with and without BSA. Addition to these solutions, P-123 micelles were obtained for drug encapsulation with solvent evaporation method and cosolvent evaporation method in DW and SBF with and without BSA. The copper grid (200 mesh) was dipped into this solution and waited for 15 seconds. In this way, STEM samples were prepared. These samples were dried under vacuum and 30^{o}C to obtain totally dry surfaces. The images of the micelles were recorded at different magnifications.

3.2.7. TEM Analysis

TEM analysis was performed by JEM - 1220 Electron Microscope. In TEM analysis, the electrons are emitted from a filament and accelerated by a high voltage and this results focus on the sample by electromagnetic fields.

Before the TEM analysis, P-123 micelles were obtained with DW with and without BSA. The copper grid (200 mesh) was dipped into this solution and waited for 15 seconds. In this way, TEM samples were prepared. These samples were dried under vacuum and 30^{o}C to obtain totally dry surfaces. The images of the micelles were recorded at different magnifications.

3.2.8. AFM Analysis

Atomic Force Microscope analysis was performed by Bruker – MultiMode Nanoscope8.

Afm measures forces between a tip and a sample and these forces are resulting from different interactions.The origin of these interactions can be ionic repulsions, van der Waals forces, capillary forces, electrostatic forces, magnetic forces, elastic deformations and plastic deformations.

The probe is placed on the end of a cantilever. The amount of force between the probe and sample is dependant on the spring constant of the cantilever and the distance between the probe and the sample surface. This force can be described using Hooke's Law (3.3) :

$$F=-k\bullet x \qquad (3.3)$$

where F is the Force, k is the spring constant, and x is the cantilever deflection.
AFM works in three modes. These modes are, contact mode, tapping mode, and non-contact mode, respectively. (Blanchard, 1996; Cappella et al., 1999).

1) Contact mode

By preserving a constant cantilever deflection, the force between the probe and the sample remains constant and an image of the surface is obtained. During this process, the force on the tip is repulsive.

Contact mode has several advantages and disadvantages. It can do fast scanning, good for rough samples, and used in friction analysis. These are some advantages of afm. Addition to these, afm has some disadvantages. For example, during contact mode measurements, forces can damage soft samples' surfaces.

2) Intermittent (Tapping) Mode

The imaging is similar to contact mode. The cantilever oscillates and the tip makes repulsive contact with the surface of the sample at the lowest point of the oscillation.

The probe lightly “taps” on the sample surface during scanning, contacting the surface at the bottom of its swing.

Tapping mode has several advantages and disadvantages. It allows high resolution of easily damaged samples and it is good for biological samples. But tapping mode needs slower scan speed.

3) Non-contact Mode

The probe does not contact the sample surface, but oscillates above the adsorbed fluid layer on the surface during scanning. Using a feedback loop to monitor changes in the amplitude due to attractive VdW forces the surface topography can be measured.

Non-contact mode has several advantages and disadvantages. Non-contact mode has very low force during topography measurement, this speciality extends afm probe’s lifetime. Non-contact mode can be used in air, fluid or vacuum environments. In vivo measurements of biological samples and chemical processes are possible to observe. At the same time, non-contact mode has poor resolution and usually needs ultra high vacuum to get best imaging. These are disadvantages of non-contact mode of afm.

Before AFM analysis, hemi micelles were obtained. It is a micelle attached to a surface. To obtain hemi micelles, first of all top layers of mica surfaces were separated. After that, mica surface was immersed in tri-block copolymer micelle solution during 15 seconds. These surfaces were put on the glass surfaces and dried during 7days at room temperature and 1 bar. To obtain AFM images, mica surface must be totally dry. For AFM analysis, P-123 surfactant micelles were obtained in DW and SBF with and without BSA. Addition to these solutions, P-123 micelles were obtained for drug encapsulation with solvent evaporation method and cosolvent evaporation method in DW and SBF with and without BSA.

CHAPTER 4

RESULTS AND DISCUSSION

4.1. The Forms of P-123 Molecules in Aqueous Solutions: Surface Tension Measurements

The forms of polymeric surfactant, P-123 molecules in aqueous solutions vary with its concentration. Therefore surface tension measurements were performed as a function of P-123 concentration and presented Figure 4.1. As seen in Figure 4.1., increasing P-123 concentration reduces the surface tension up to a certain concentration. That is, surface tension reaches a constant value, CMC, which does not vary with a further increase in surfactant concentration.

The surface tension decreased from an initial value of 72 mN/m to a value of about 33 mN/m at a concentration of $2x10^{-4}$ M. Based on the results given above, a schematic representation of the changes in surface tension as a function of concentration is given in the inset figure. The surface tension behavior of P-123 could be divided into three concentration regions marked as Regions I, II and III (Figure 4.1.). Region I is believed to consist principally of monomers whereas Region III involves fully developed micelles. Region II is a region where surfactant molecules start to form dimers and trimers and the decrease in surface tension is low. The adsorption density may be calculated from the slope of Region I where surface tension decreases linearly, by using the Gibbs equation.

$$\Gamma=-1/RT(d\Upsilon/d\ln C) \qquad (4.1)$$

where Γ and C are the surface excess and the bulk concentration of the surfactant component. The area per molecule at the interface, A, can be calculated as (4.2):

$$A=1/\Gamma N_{av} \qquad (4.2)$$

where Γ is the surface excess concentration at monolayer coverage and N_{av} is the Avogadro's number. The area calculated provides information on the degree of packing and the orientation of the adsorbed molecule.

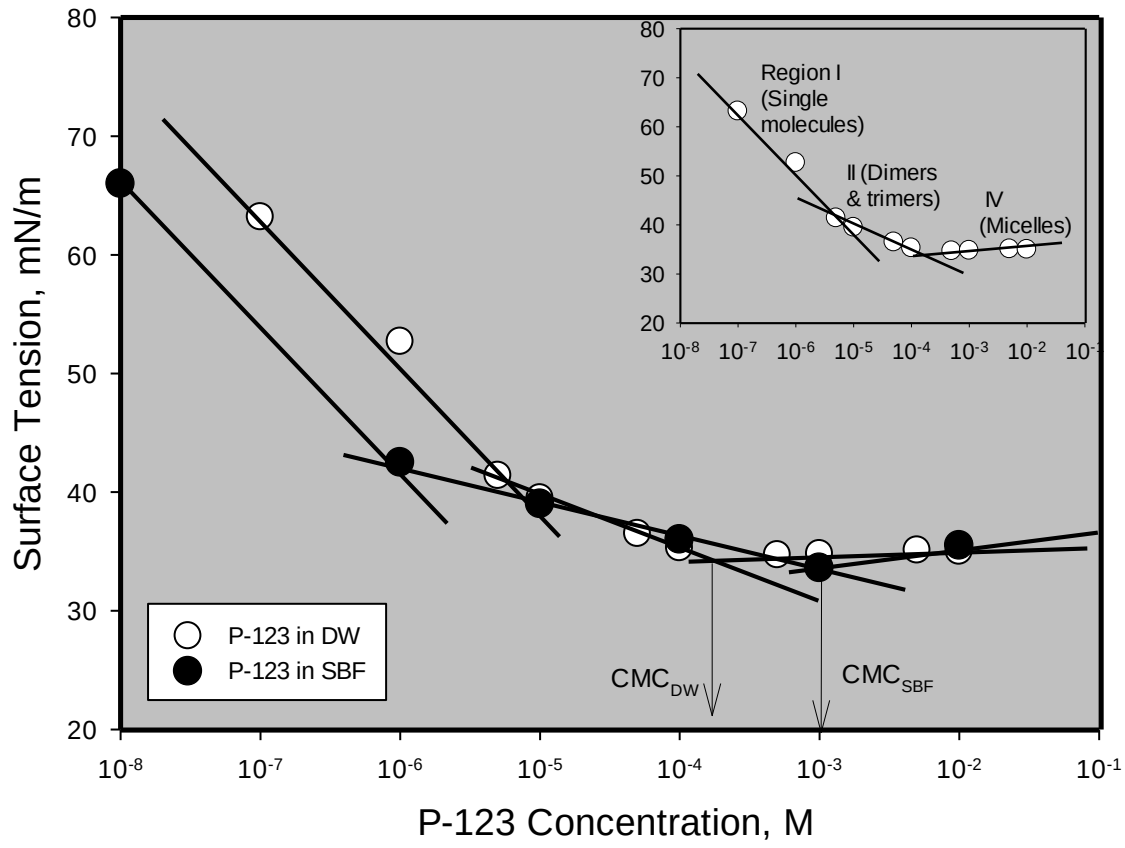

Figure 4.1. Surface tension results of P-123 in DW and SBF.

From the surface tension measurements given in the above paragraphs, the adsorption density was calculated to be 2.057×10^{-10} moles/cm^2. This corresponds to a parking area of about 0.807 nm^2 per molecule of P-123.

Similar type of surface tension measurements were also conducted in SBF and presented in the same figure (Figure 4.1). As it is seen from the figure that the surface tension values are lower in SBF in Region I and same in Region II and III. However, the concentrations where dimers-trimers (first break in the curve) and micelles (second break in the curve, CMC) form are lower in SBF.

4.2. Characterization of P-123 Micelles in Water

4.2.1. Size of P-123 Micelles: AFM, DLS, STEM, TEM

Size analysis of P-123 micelles were presented in the following figures. As it seen from the AFM, STEM, TEM images and DLS measurements that the size of micelles are around 18 nm at 10^{-4} and 10^{-2} M concentrations and increase little (20 nm) at 10^{-3} M concentration. At 10^{-2} M concentration, on the other hand, the size of micelles are little small due to the transformations in the spherical structures of micelles to the cylindirical forms (Petrov et al., 2008). These results were also confirmed by the images of STEM and TEM images and DLS measurements.

Based on the results given above, 10^{-3} M P-123 concentration was chosen for the all the experimental studies. Because, the formation of micelles start at 10^{-4} M but this concentration is too low to make perfect spherical and tight micelles. 10^{-2} M, on the other hand, the concentration is too high to keep their shapes spherical.

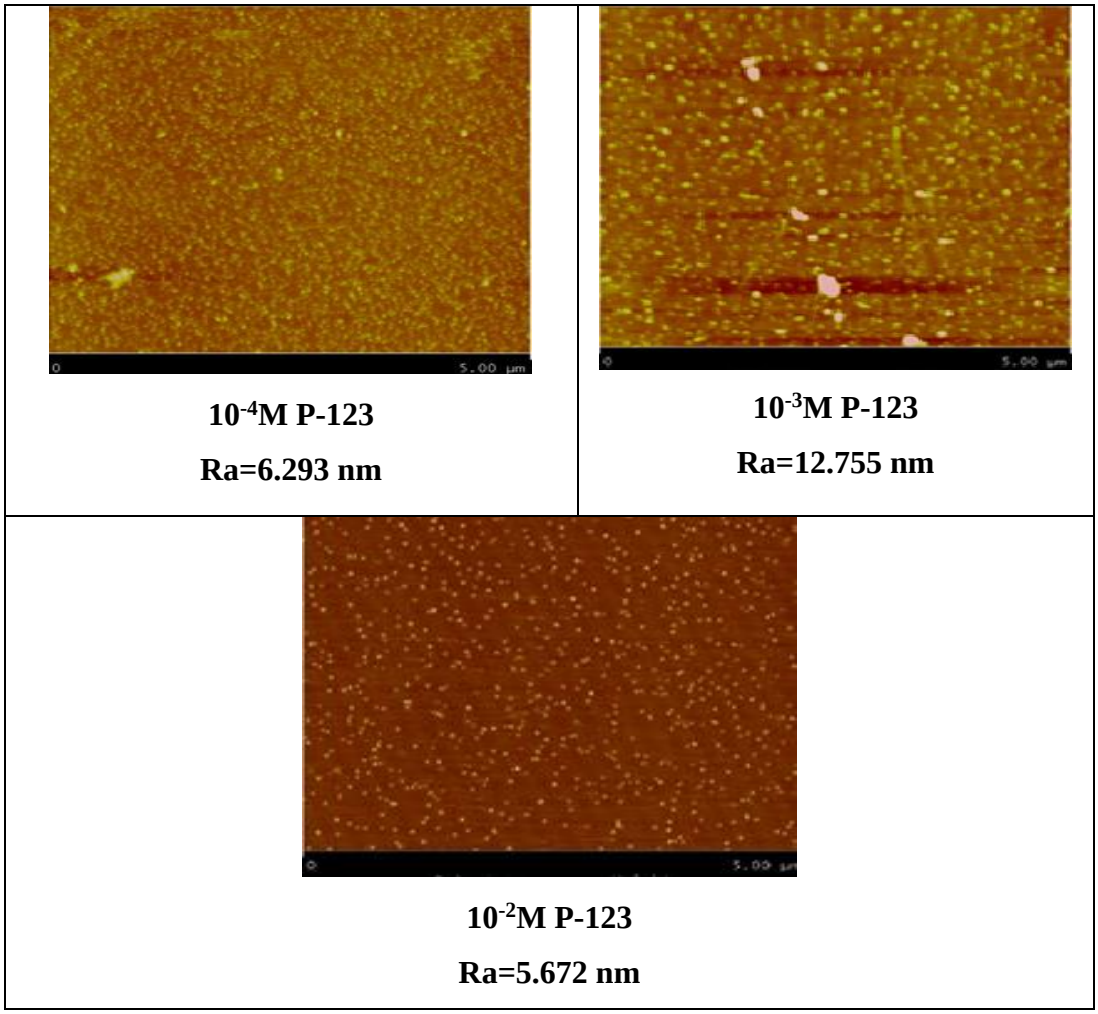

Figure 4.2. AFM images of P-123 micelles in DW at different concentrations.

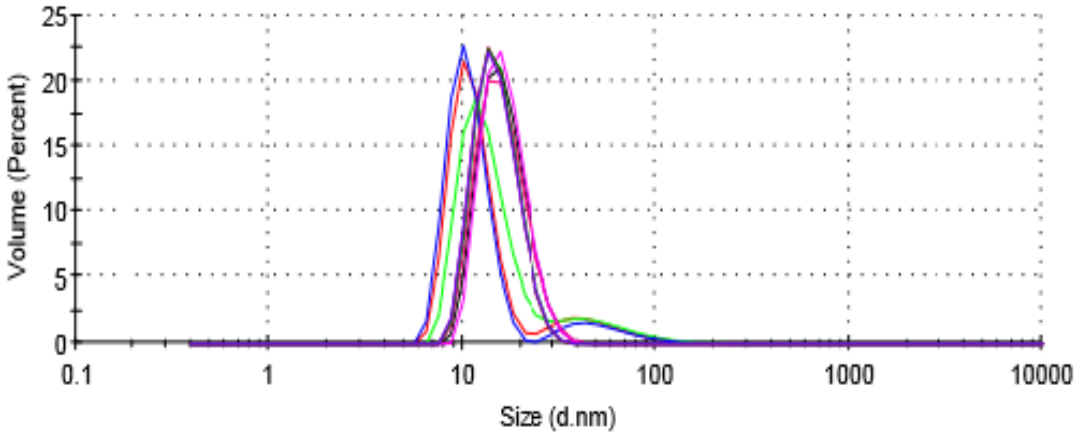

Figure 4.3. DLS results of P-123 micelles at different concentrations in DW.

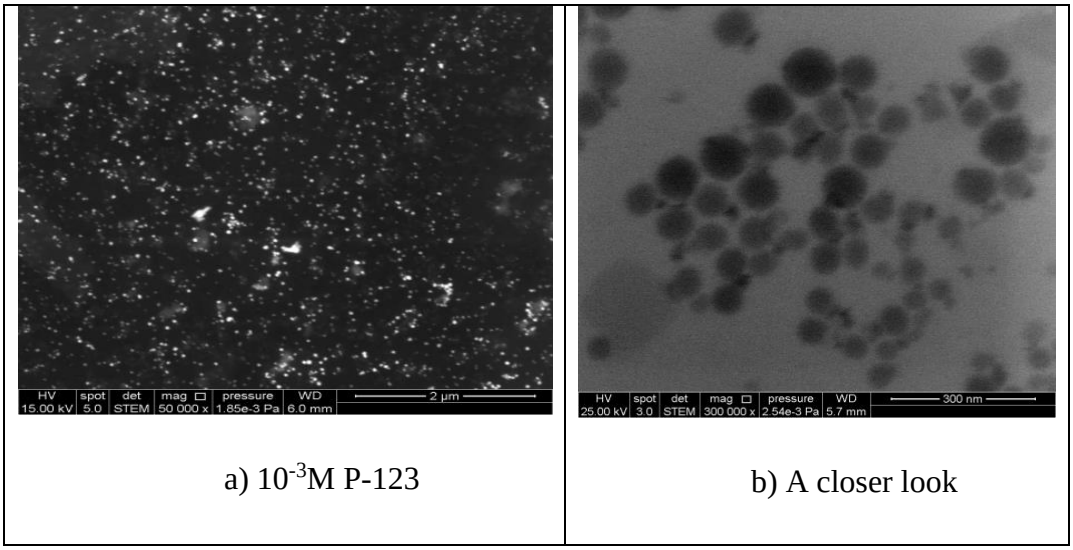

a) 10^{-3}M P-123 b) A closer look

Figure 4.4. STEM images of P-123 micelles at 10^{-3} M in DW at different magnifications a) x50.000 b) x300.000.

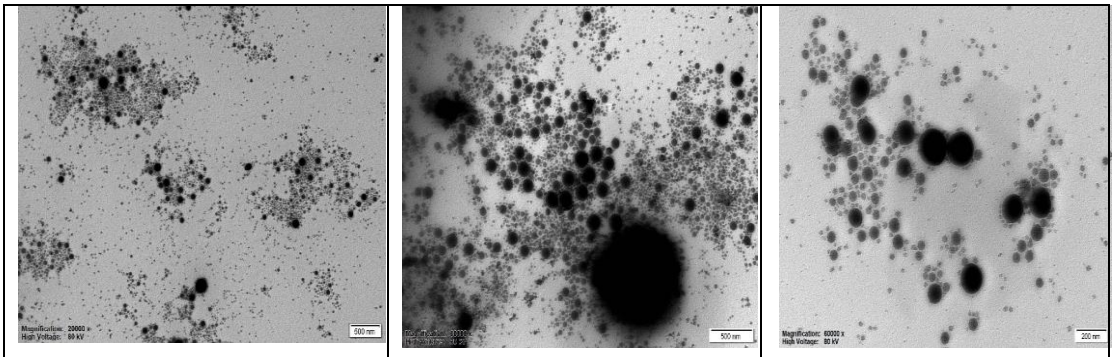

a) 10^{-3} M P-123 b) A closer look c) A closer look

Figure 4.5. TEM images of P-123 micelles at 10^{-3} M in DW at different magnifications a) x20.000 b) x30.000 c) 60.000.

4.2.2. Charge of P-123 Micelles: Zeta Potential Measurements

Zeta potential measurements of P-123 micelles at different concentrations of P-123 (10^{-4}, 10^{-3} and 10^{-2} M) were conducted and given in Figure 4.6.. As it is seen from the Figure 4.6., the charge distribution of micelles change depending on concentration. At 10^{-4} and 10^{-3} M concentrations, the charge distribution is broad and there are both negatively and positively charged micelles in the solution (Jones et al., 1999). At 10^{-2} M, on the other hand, the distribution becomes narrow and negative.

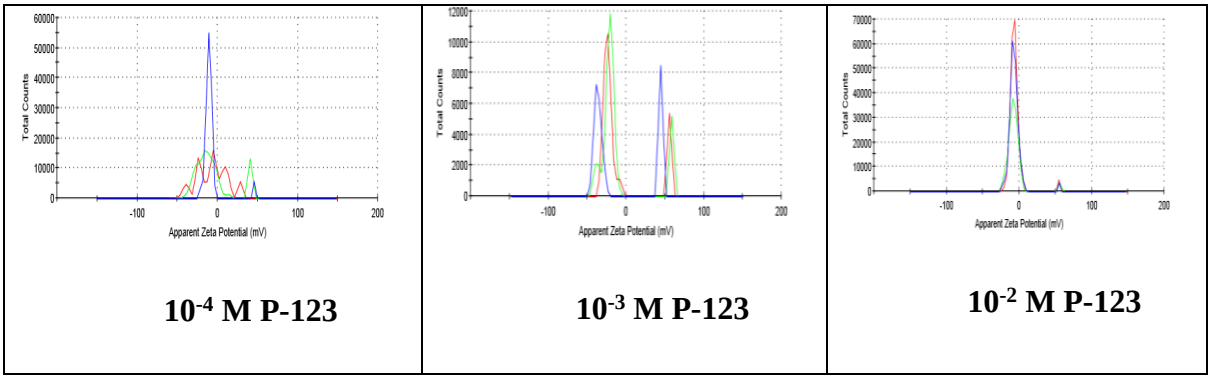

Figure 4.6. Charge of P-123 micelles at different concentrations in DW.

4.3. Characterization of BSA in Water

Some experiments were conducted to characterize BSA in water and the results of these studies were presented in Figure 4.7. As it is seen from the DLS results, size of BSA molecules are around 5-6 nm. Which is most probably the folded form of BSA molecules. AFM results, on the other hand, was different and gave much higher values. This could be due to the preparation method where molecules are attached on mica surface and let dry for AFM measurements. Since the mica surface is hydrophobic, the placement of BSA molecules on the surface will depend on their structure. BSA molecules may cover larger area. Therefore one may expect larger apperance of molecules on these surfaces. This can not be compared directly with other results. STEM results were good images and clear. They also look larger compare to the DLS results. This might be again because of sample preparation method where molecules were left to dry on a hydrophobic carbon surface.

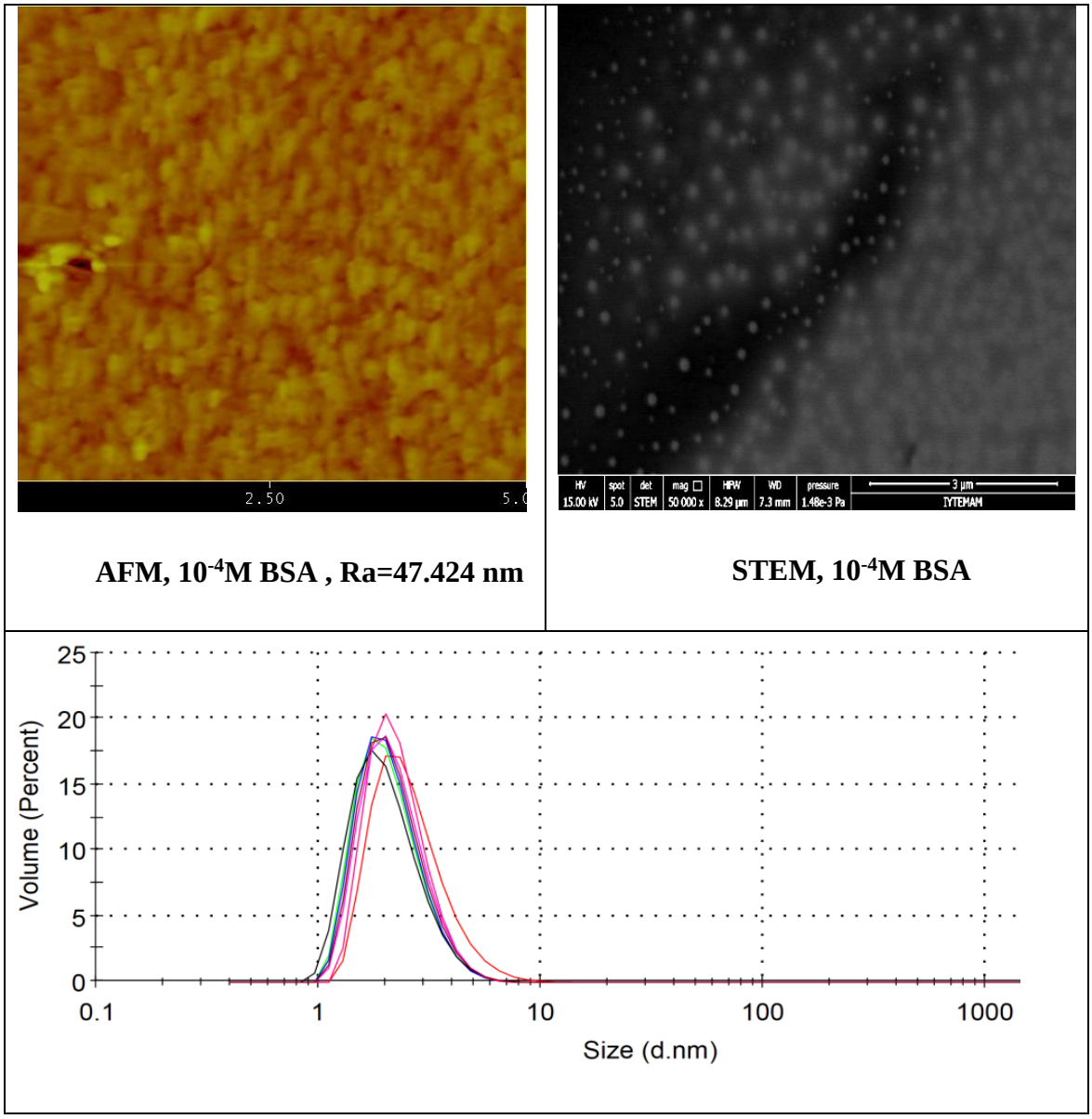

Figure 4.7. Characterization of BSA in water.

4.4. Characterization of P-123 Micelles in the Presence of BSA in Water

4.4.1. Size of Micelles: AFM, DLS, STEM, TEM

Similarly the size analysis of P-123 micelles at 10^{-3} M concentration in the presence of 10^{-4} M were presented in the following figures. As it seen from the AFM, STEM, TEM images and DLS results that the size of micelles seem to not change and stay around 20 nm. However, some BSA structures form around micelles and bring micelles together that may show micelles larger as obtained by AFM, STEM and TEM. The images of TEM and STEM

also shows that the actuall size of micelle do not change but they come together in the presence of BSA. This might be due to the preparation method (evaporation of water on mica surface for AFM and on carbon surface for STEM and TEM) used for the measurements in the presence of BSA. The protein addition was after formation of micelles due to represent the body conditions. In which P-123 micelles loaded with drug was introduced into the body fluid which carry albumine.

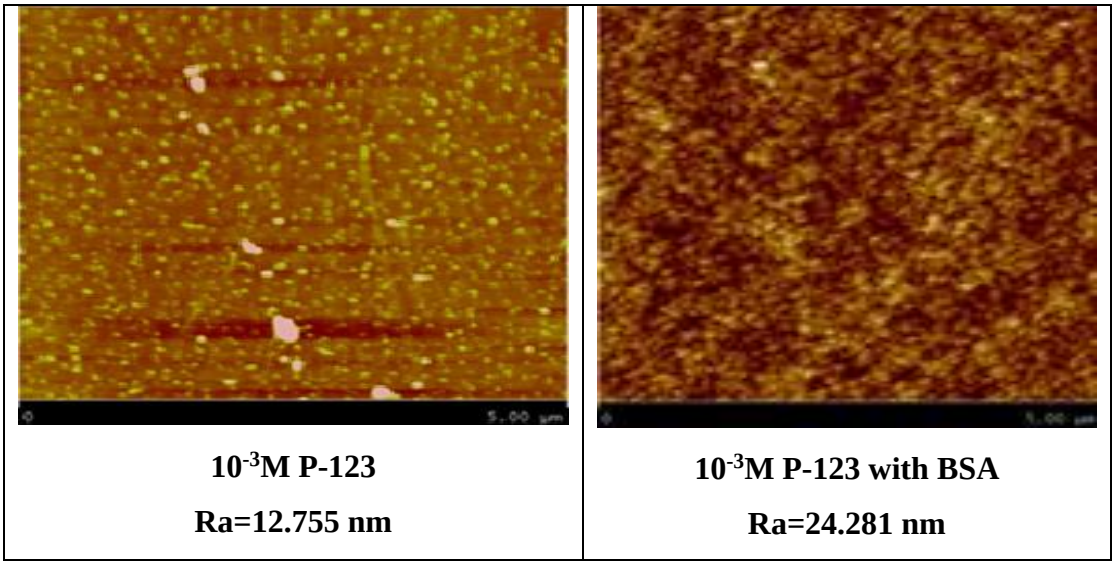

10^{-3}M P-123

Ra=12.755 nm

10^{-3}M P-123 with BSA

Ra=24.281 nm

Figure 4.8. AFM images of P-123 micelles in the absence and presence of BSA in DW.

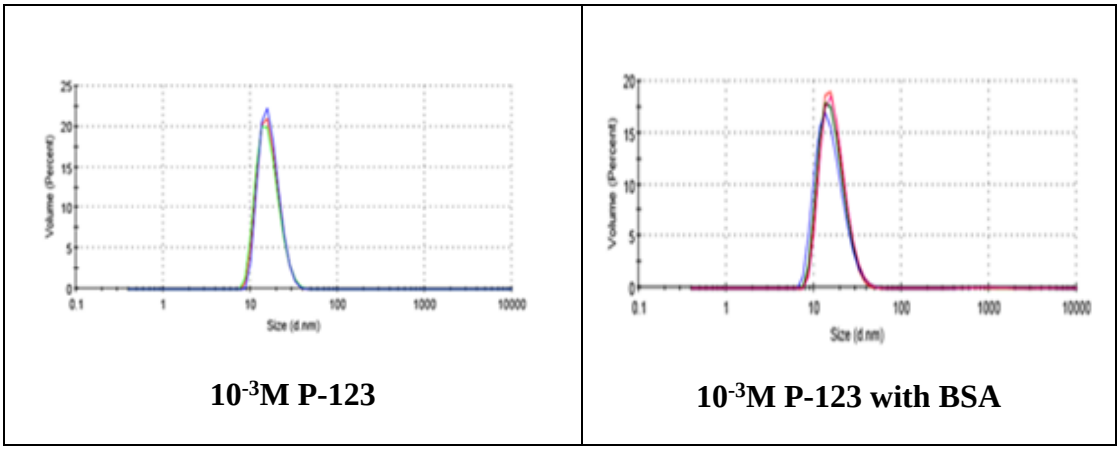

10^{-3}M P-123

10^{-3}M P-123 with BSA

Figure 4.9. DLS results of P-123 micelles in the absence and presence of BSA in DW.

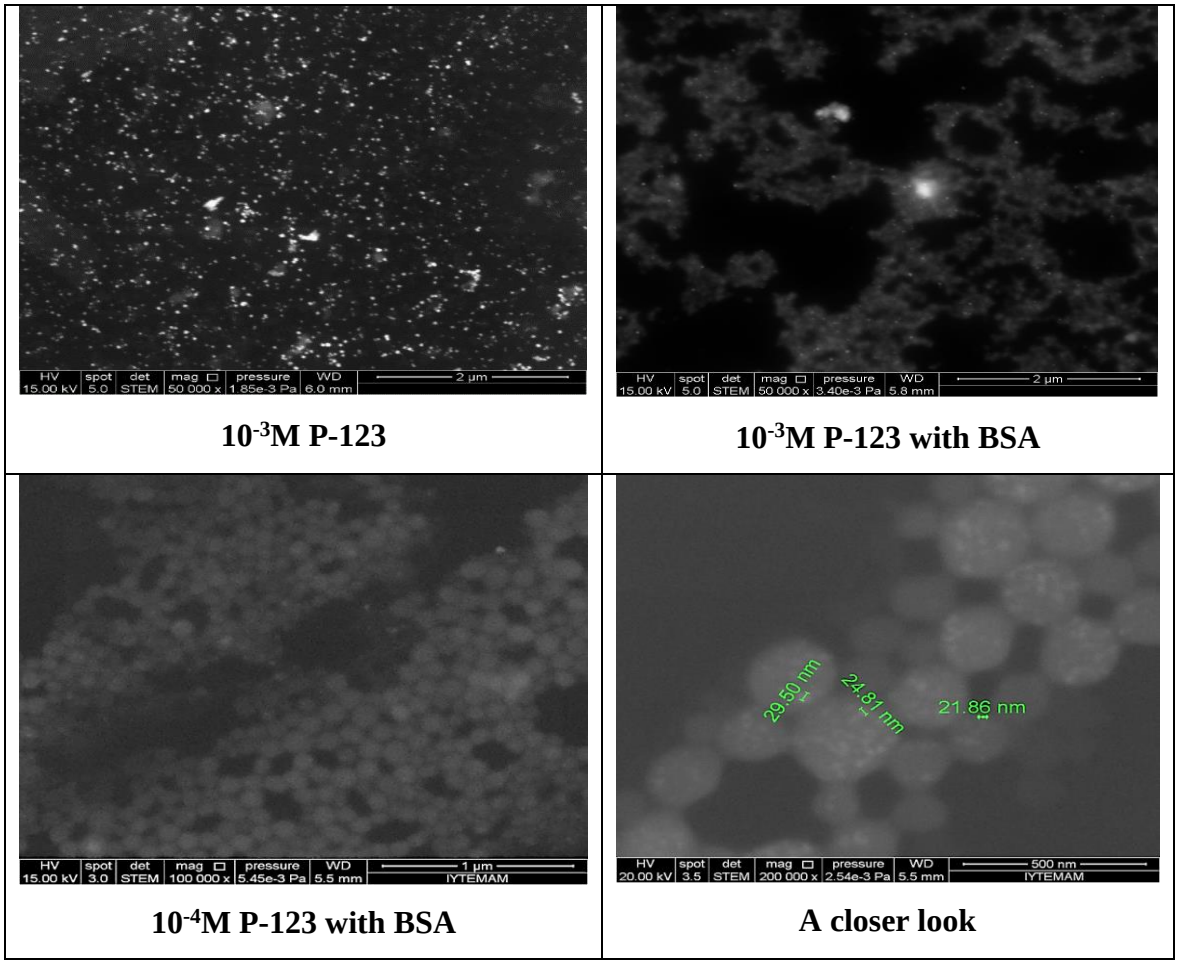

10^{-3}M P-123 | **10^{-3}M P-123 with BSA**

10^{-4}M P-123 with BSA | **A closer look**

Figure 4.10. STEM images of P-123 micelles in the absence and presence of BSA in DW.

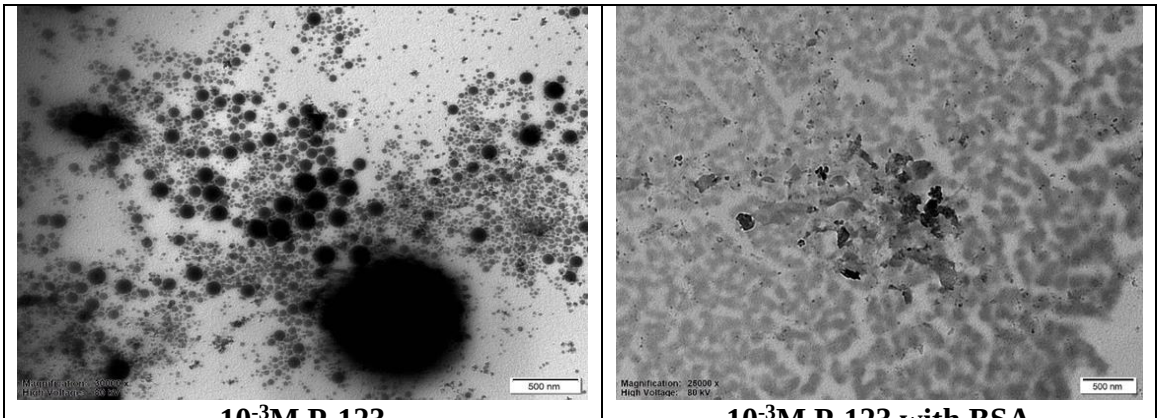

10^{-3}M P-123 | **10^{-3}M P-123 with BSA**

Figure 4.11. TEM images of P-123 micelles in the absence and presence of BSA in DW.

4.4.2. Charge of P-123 Micelles in the Presence of BSA: Zeta Potential Measurements

Zeta potential measurements of P-123 micelles at 10^{-3} M concentration of P-123 were conducted in the presence of BSA at 10^{-4} M concentration and given in Figure 4.12.. As it is seen from the Figure 4.12., the charge distribution of micelles change in the presence of BSA. The broad charge distribution becomes narrow and neutral (distribution is around zero charge). This might be due to the shielding effect of BSA around micelles. However, one has to be careful about the usage of these results. This charge can not be used to explain the interactions or agglomerations among molecules/micelles and compared with the size results or images obtained from different devices such as AFM, STEM and TEM where water is evaporeted. Because these measurements are in water.

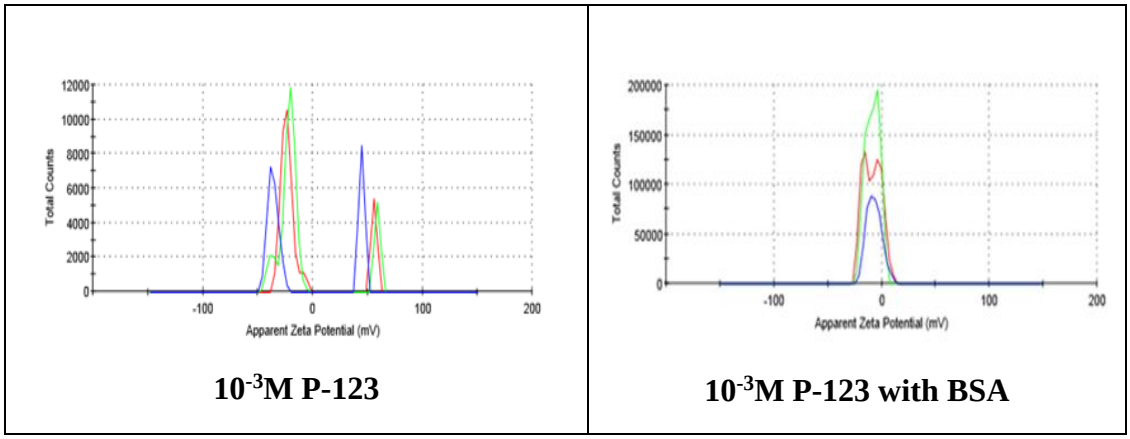

10^{-3}M P-123 **10^{-3}M P-123 with BSA**

Figure 4.12. Charge of P-123 micelles in the absence and presence of BSA in DW.

4.5. Characterization of P-123 Micelles in SBF

Similar type of characterization studies (AFM, DLS, STEM) conducted in DW were also carried out in SBF and the results are presented in Figures (4.13-4.15). As it seen the micelle structures became together to form loose and large aggregates in SBF. These structures were observed both by AFM and STEM methods. The DLS results, on the other hand, showed no change and gave similar sizes (around 20 nm). Again this

might be due to the preparation method where samples are dried on mica and carbon surfaces or settling of larger aggregates in DLS and leaving the solution with free micelles.

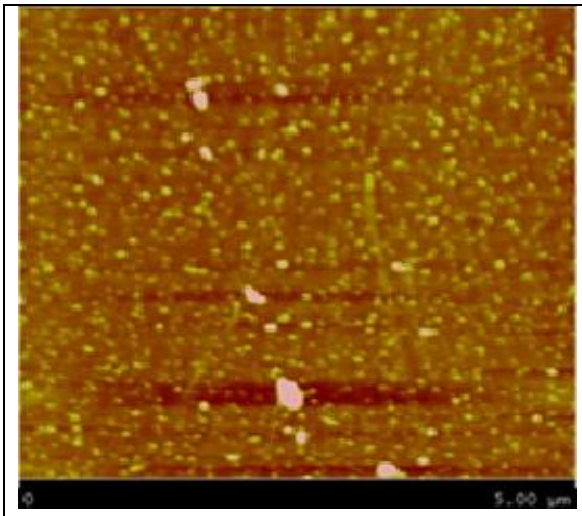

10^{-3}M P-123 in DW

Ra=12.755 nm

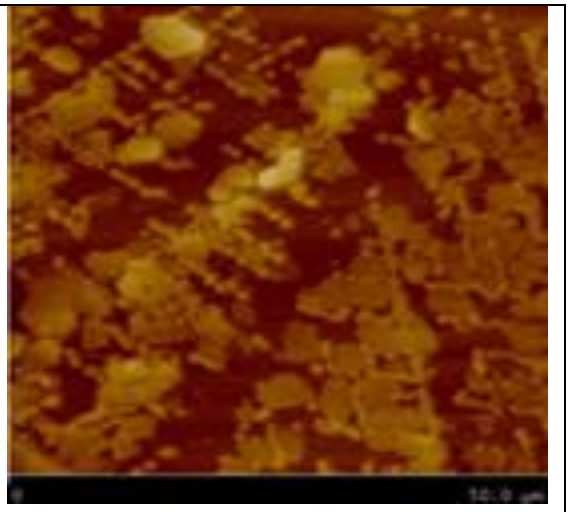

10^{-3}M P-123 in SBF

Ra=2.221 µm

Figure 4.13. AFM images of P-123 micelles at 10^{-3} M in DW and SBF.

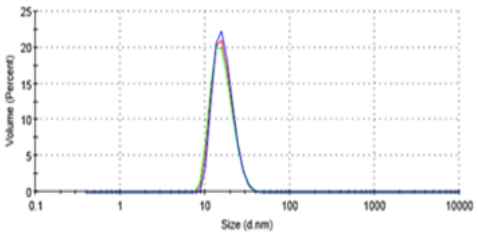

10^{-3}M P-123 in DW

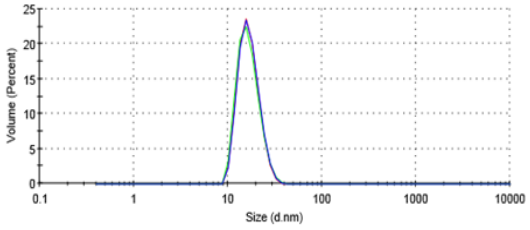

10^{-3}M P-123 in SBF

Figure 4.14. DLS results of P-123 micelles at 10^{-3} M in DW and SBF.

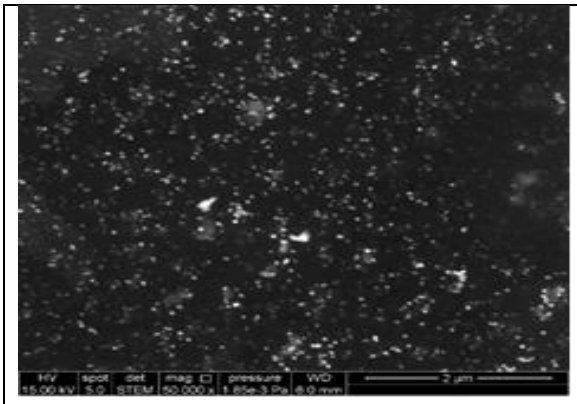

10^{-3}M P-123 in DW

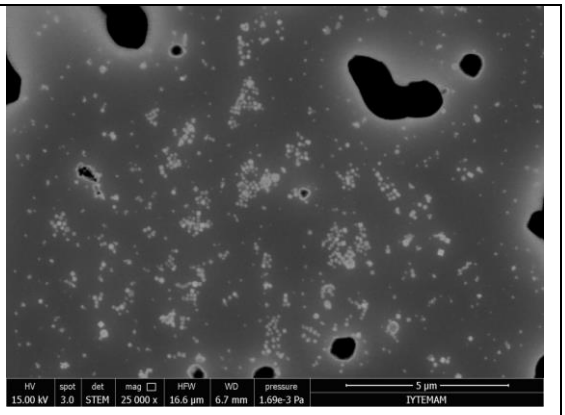

10^{-3}M P-123 in SBF

Figure 4.15. STEM images of P-123 micelles at 10^{-3} M in DW and SBF.

Zeta potential measurements of P-123 micelles (10^{-3} M) in SBF with and without BSA could not be performed due to the loose aggregation in the system as seen in STEM images.

4.6. Characterization of P-123 Micelles in the Presence of BSA in SBF

Chracterization studies (AFM, DLS, STEM) conducted in DW were also carried out in SBF in the presence of BSA and the results are presented in Figures (4.16-4.18). As it was observed for the micelle structures in SBF without BSA, there were large and loose aggregates in the presence of BSA in SBF. Similarly, these structures were observed both by AFM and STEM methods. The DLS results, on the other hand, again showed no change and gave similar sizes (around 20 nm). This could be explained by the same argument given above for measurements.

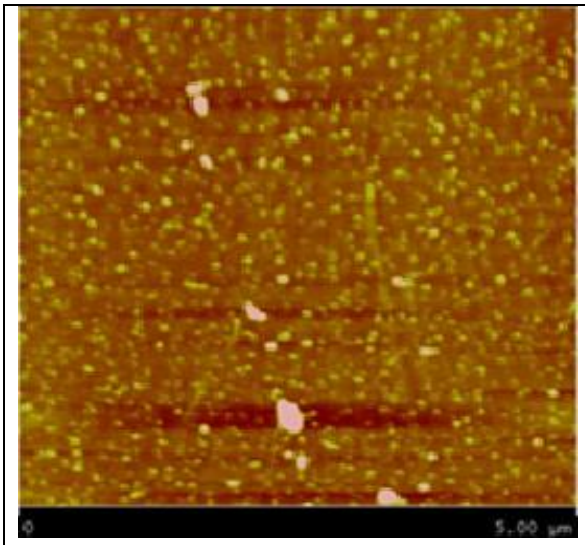

10^{-3}M P-123 in DW

Ra=12.755 nm

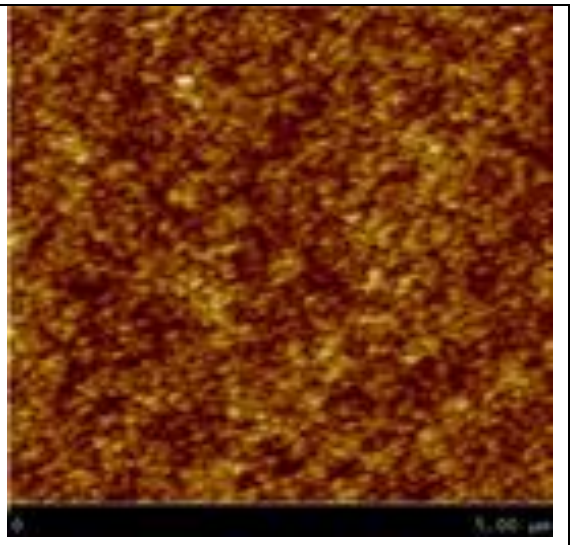

10^{-3}M P-123 with BSA in DW

Ra=24.281 nm

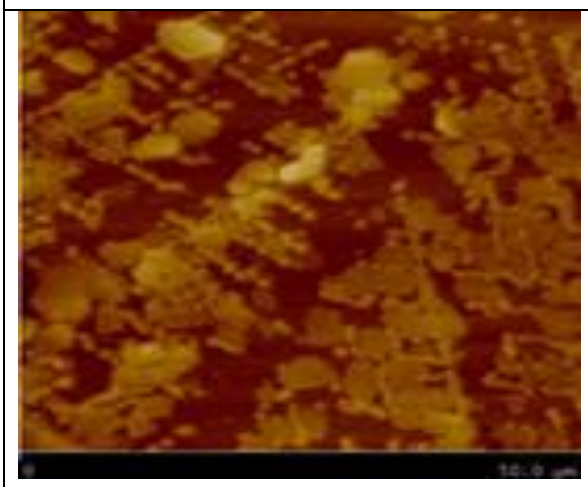

10^{-3}M P-123 in SBF

Ra=2.221 µm

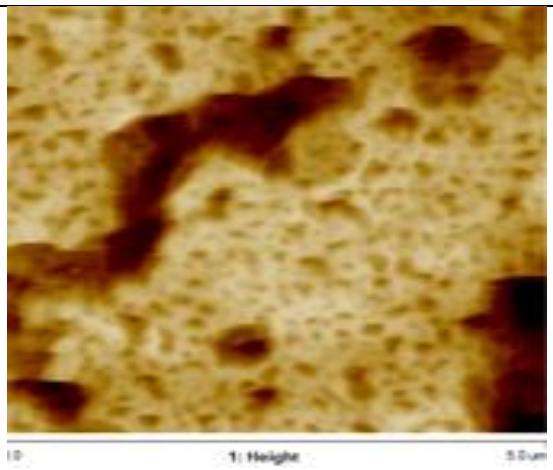

10^{-3}M P-123 with BSA in SBF

Ra= 141 nm

Figure 4.16. AFM images of P-123 micelles at 10^{-3} M in the absence and presence of BSA in DW and SBF.

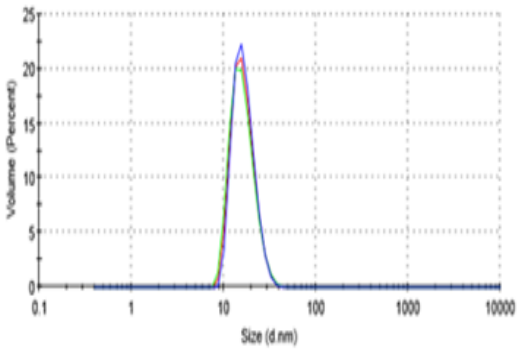

10^{-3}M P-123 in DW

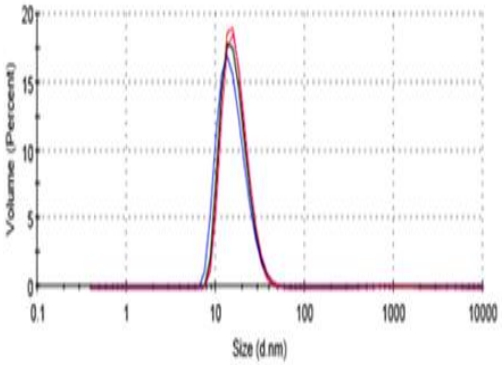

10^{-3}M P-123 with BSA in DW

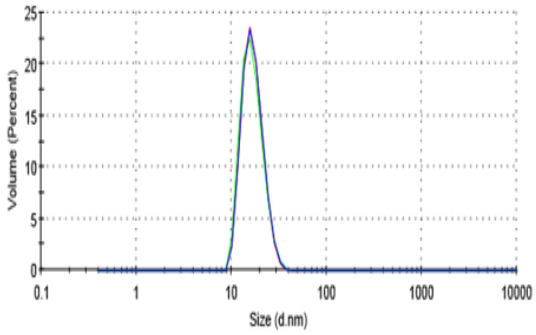

10^{-3}M P-123 in SBF

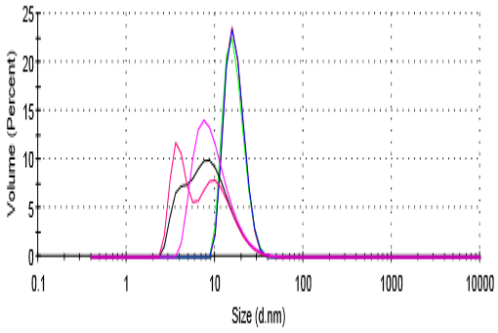

10^{-3}M P-123 with BSA in SBF

Figure 4.17. DLS results of P-123 micelles in the absence and presence of BSA in DW and SBF.

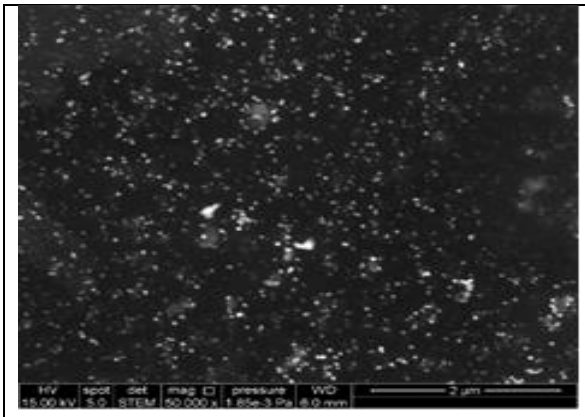

10^{-3}M P-123 in DW

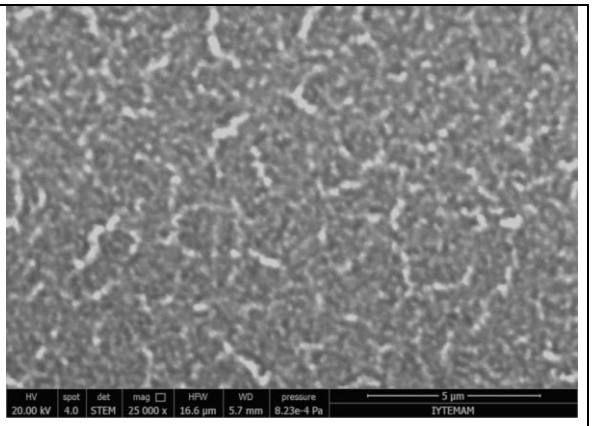

10^{-3}M P-123 with BSA in DW

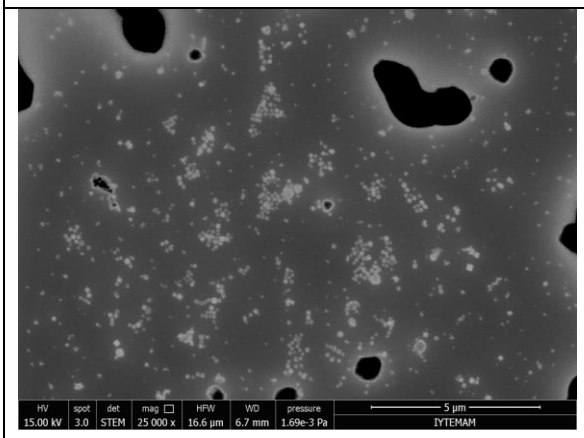

10^{-3}M P-123 in SBF

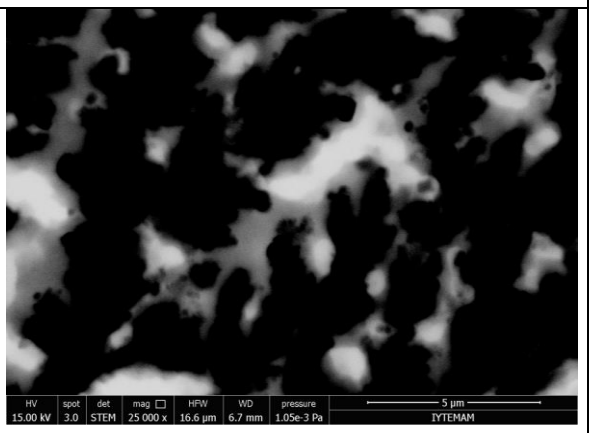

10^{-3}M P-123 with BSA in SBF

Figure 4.18. STEM images of P-123 micelles in the absence and presence of BSA in DW and SBF.

Zeta potential measurements of P-123 micelles (10^{-3} M) in SBF with and without BSA could not be performed due to the loose aggregation in the system as seen in STEM images.

4.7. Characterization of Micelles Loaded with Drug in Water

Size analysis of P-123 micelles at 10^{-3} M concentration loaded with drug in water by solvent evaporation method were presented in the following figures. The results of co-solvent evaporation method, on the other hand, had some problems during the evaporation process. Therefore the results of co-solvent evaporation method are not presented here. As it seen from the DLS results (Figure 4.19) that the size of micelles seem to not change and stay around 20 nm in the presence of drug. The STEM results, on the other hand, show some increase in the size of micelles when they loaded with drug (Figure 4.20). One can also observe some agglomeration among micelles which might be the reason for the different results of DLS.

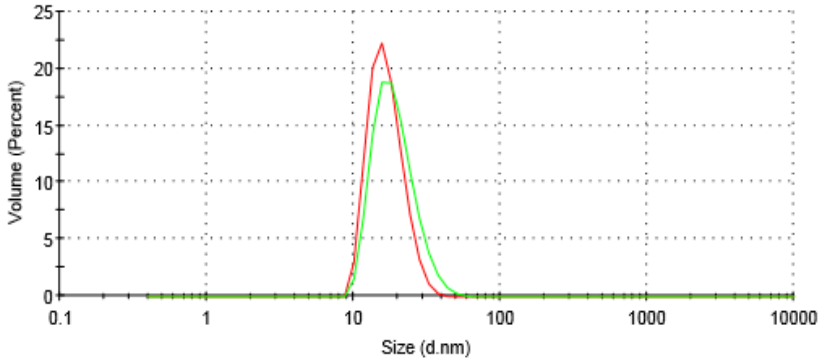

Solvent evaporation method

Figure 4.19. DLS results of P-123 micelles with evaporation methods in DW.

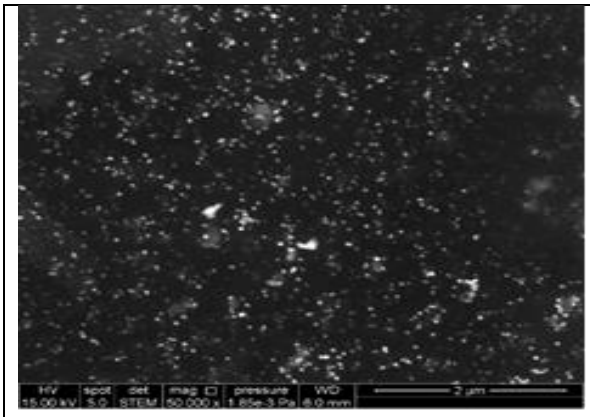

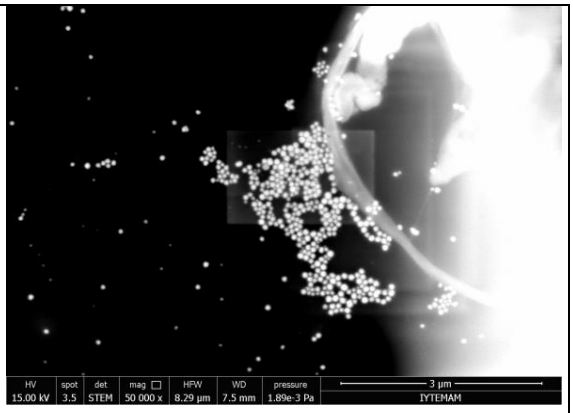

10^{-3}M P-123 | **Solvent evaporation method**

Figure 4.20. STEM images of only P-123 micelles at 10^{-3} M P-123 micelles loaded with drug with solvent evaporation method in DW.

Zeta potential measurements of P-123 micelles at 10^{-3} M concentration loaded with drug in water by solvent evaporation method are presented in Figure 4.21. As it is seen from the figures that the charge distribution of micelles get broader in the case of evaporation method. There are both negatively and positively charged micelles in the solution.

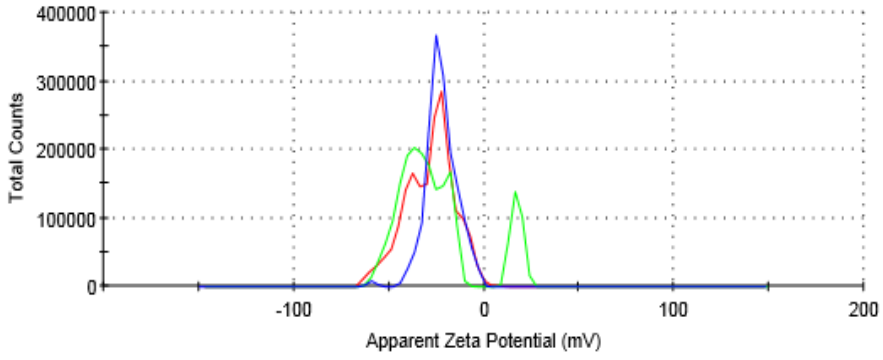

Solvent evaporation method

Figure 4.21. Charge of P-123 micelles with evaporation methods in DW.

4.8. Characterization of Micelles Loaded with Drug in the Presence of BSA in Water

Similarly the size analysis of P-123 micelles at 10^{-3} M concentration loaded with drug in water by solvent evaporation method in the presence of BSA were presented in the following figures (Figure 4.22). As it seen from the DLS results that the size of micelles seem to not change and stay around 20 nm. However, in STEM results, some BSA structures form around micelles and they bring micelles together to form large and loose aggregates.

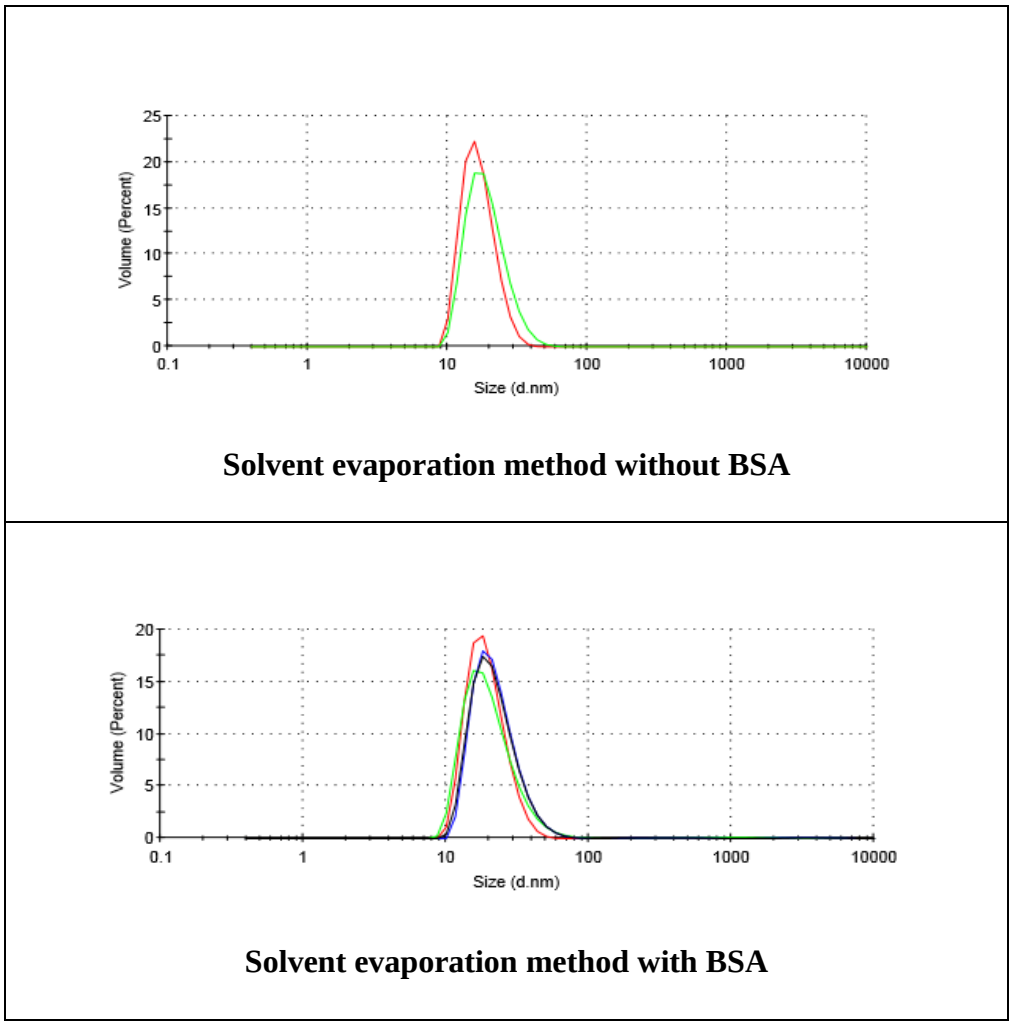

Figure 4.22. DLS results of P-123 micelles loaded with drug in the absence and presence of BSA in DW.

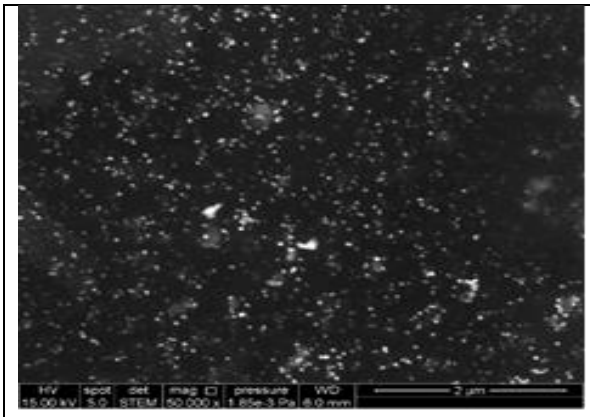

10^{-3}M P-123

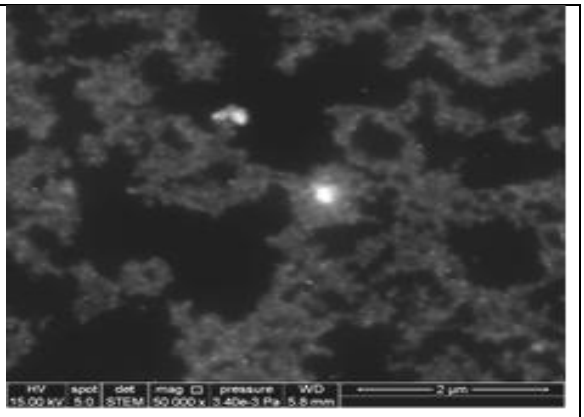

10^{-3}M P-123 with BSA

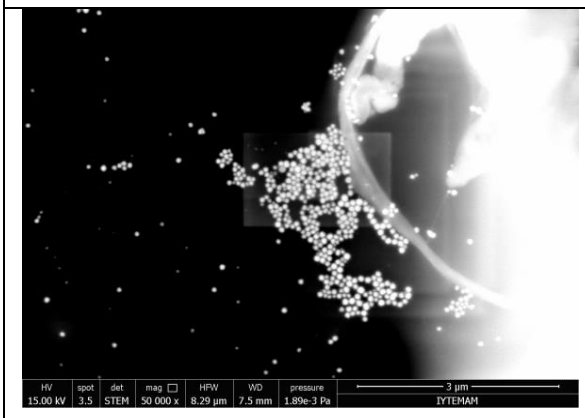

Solvent evaporation method

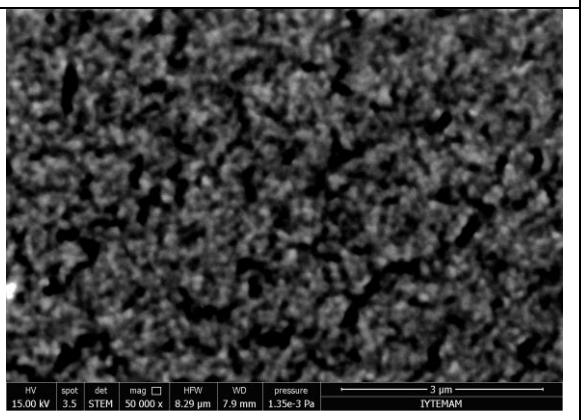

Solvent evaporation method with BSA

Figure 4.23. STEM images of P-123 micelles at 10^{-3} M and P-123 micelles loaded with drug with solvent evaporation method in the absence and presence of BSA in DW.

Zeta potential measurements of P-123 micelles at 10^{-3} M concentration loaded with drug in water by solvent evaporation method were conducted in the presence of BSA at 10^{-4} M concentration and given in Figure 4.24. As it is seen from the figure that the charge distribution of micelles change in the presence of BSA. The broad charge distribution becomes narrow and neutral (distribution is around zero charge). This might be due to the shielding effect of BSA around micelles.

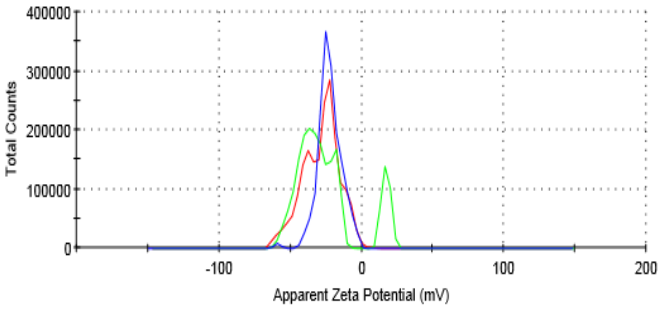

Solvent evaporation method without BSA

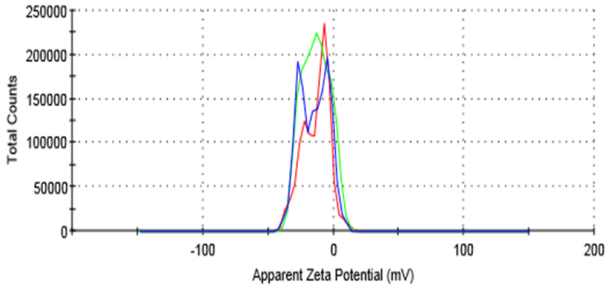

Solvent evaporation method with BSA

Figure 4.24. Charge of P-123 micelles loaded with drug in the absence and presence of BSA in DW.

4.9. Characterization of Micelles Loaded with Drug in SBF

Similar type of characterization studies (DLS, STEM) were used for size analysis of P-123 micelles at 10^{-3} M concentration loaded with drug by solvent evaporation method in SBF and the results are presented in Figures (4.25-4.26). As it is seen the micelle structures became together to form large aggregates in SBF. These structures were observed by STEM method. The DLS results, on the other hand, showed no change and gave similar sizes (around 20 nm).

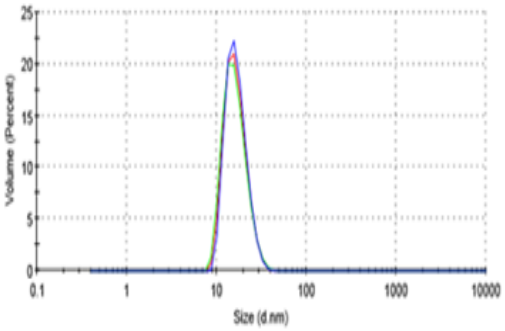

10^{-3}M P-123 in DW

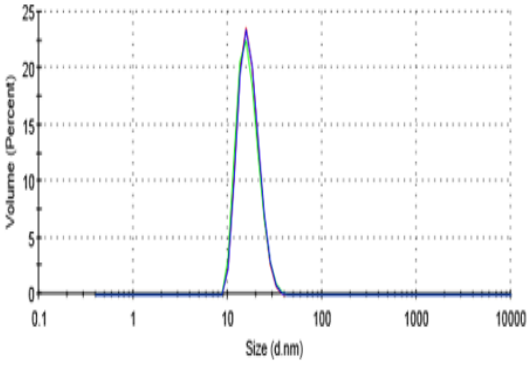

10^{-3}M P-123 in SBF

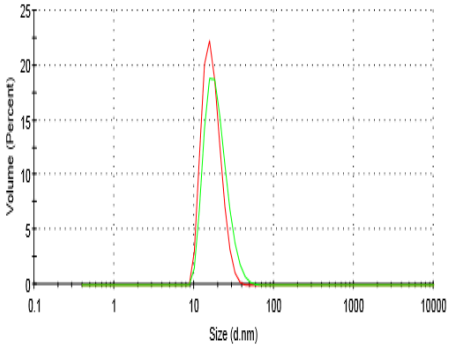

Solvent evaporation method in DW

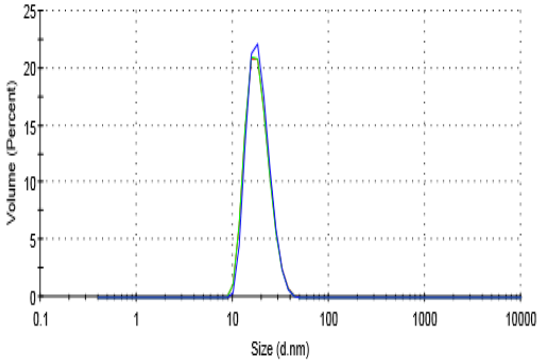

Solvent evaporation method in SBF

Figure 4.25. DLS results of P-123 micelles and P-123 micelles loaded with drug with solvent evaporation method in DW and SBF.

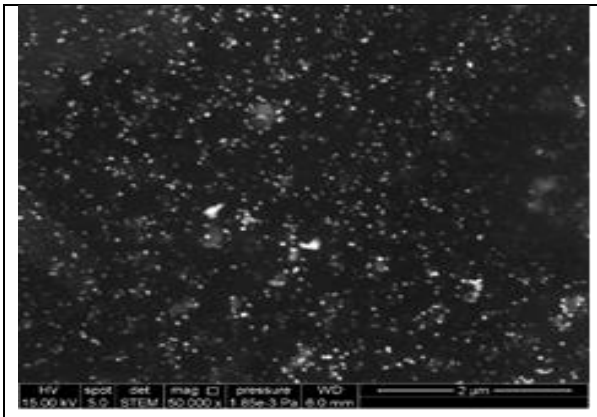

10^{-3}M P-123 in DW

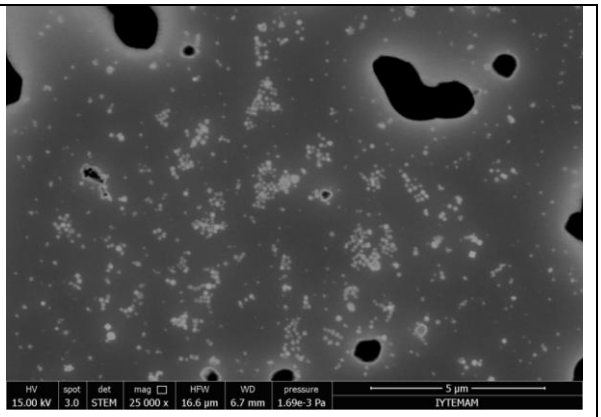

10^{-3}M P-123 in SBF

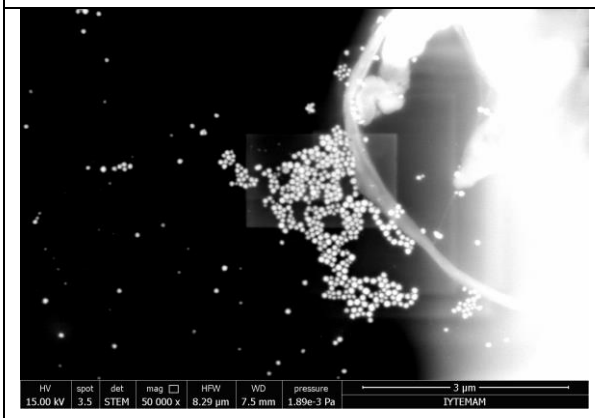

Solvent evaporation method in DW

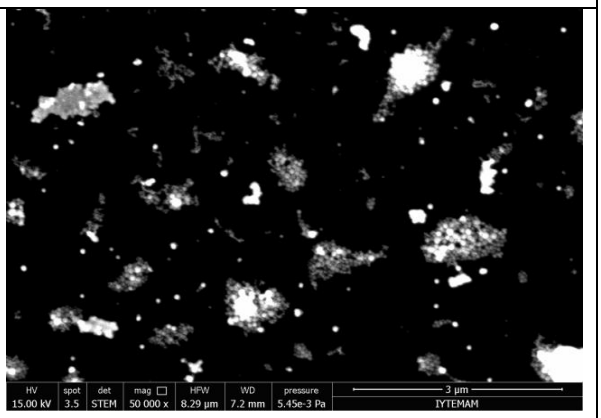

Solvent evaporation method in SBF

Figure 4.26. STEM images of only P-123 micelles and P-123 micelles loaded with drug in DW and SBF.

4.10. Characterization of Micelles Loaded with Drug in the Presence of BSA in SBF

Similar type of characterization studies (DLS, STEM) were used for size analysis of P-123 micelles at 10^{-3} M concentration loaded with drug in water by solvent evaporation method in the presence of BSA in SBF and the results are presented in Figures (4.27-4.28). In the absence of BSA the large and loose aggregates of micelles loaded with drug were observed in SBF by STEM method. In the presence of BSA,

however, some micelles looks like more dispersed. The DLS results also show a broader size distribution in this case and confirm the results of STEM.

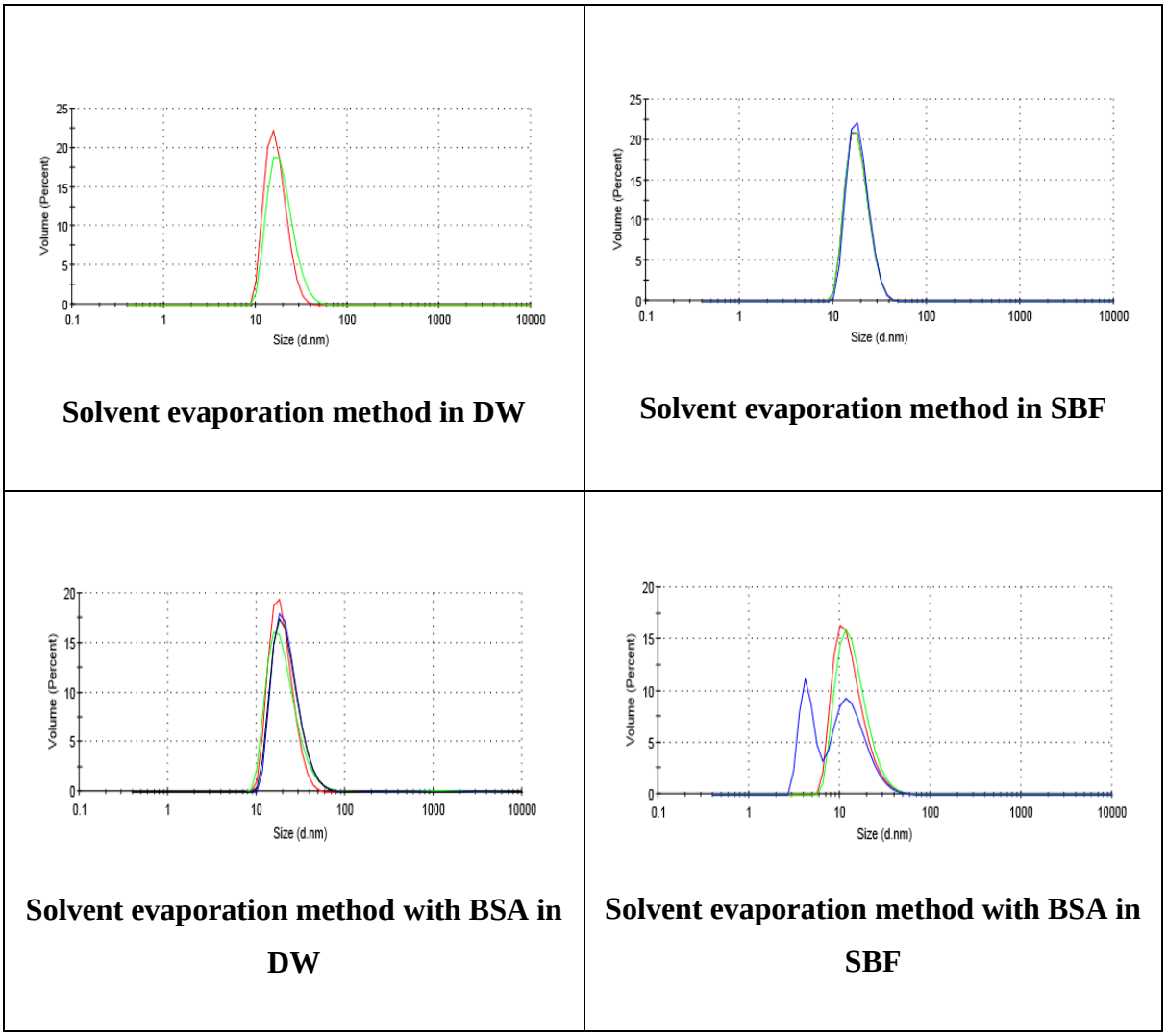

Figure 4.27. DLS results of P-123 micelles loaded with drug in the absence and presence of BSA in DW and SBF.

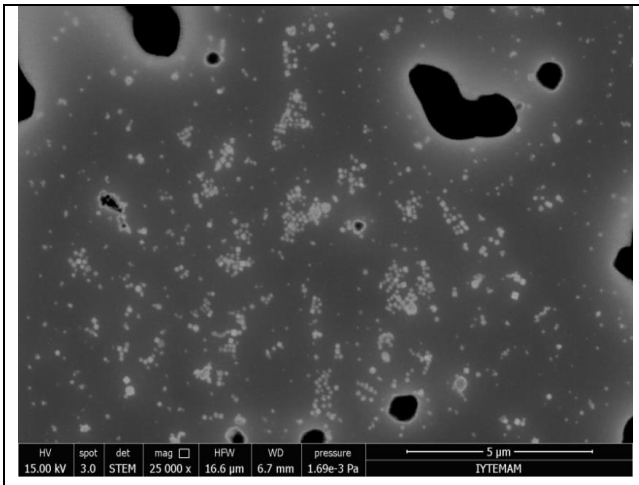

10^{-3}M P-123 in SBF

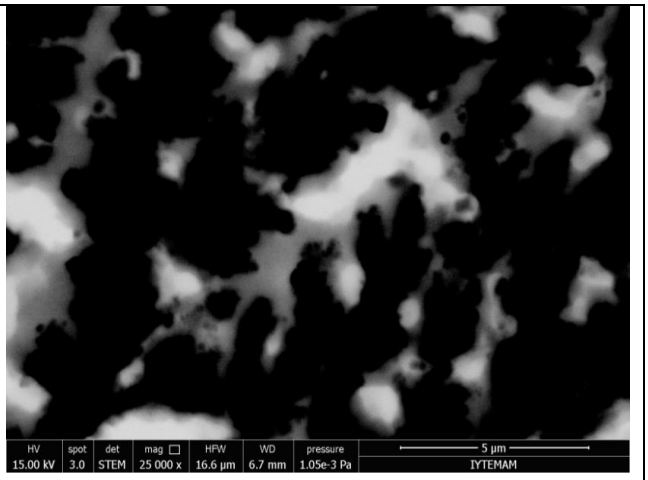

10^{-3}M P-123 with BSA in SBF

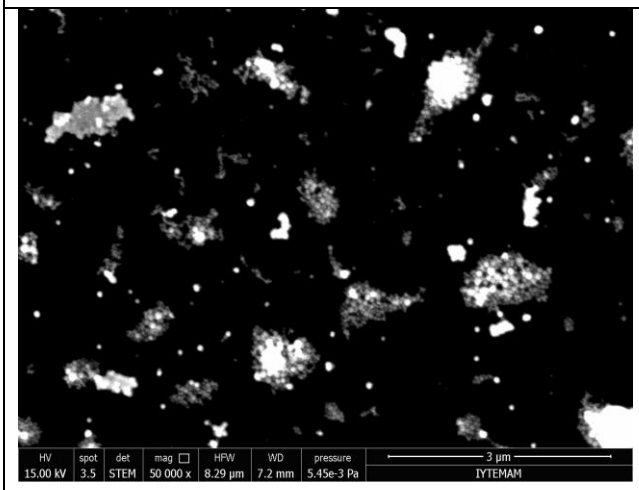

Solvent evaporation method in SBF

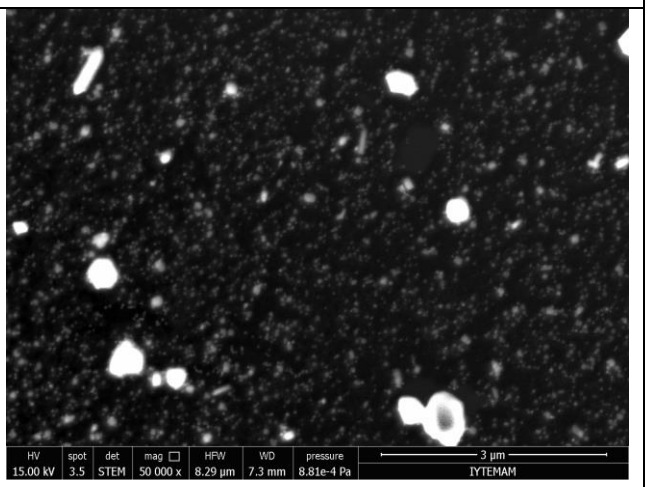

Solvent evaporation method with BSA in SBF

Figure 4.28. STEM images of P-123 micelles loaded and unloaded with drug in the absence and presence of BSA in SBF.

CHAPTER 5

CONCLUSIONS

The purpose of this study was to do full characterization of P-123 micelle structures that are commonly used as drug carriers, in the presence of BSA in water and in SBF. For this purpose several characterization methods such as AFM, DLS, STEM, and TEM were used and elucidated together to analyse the morphological changes in their structure. Surface tension measurements of P-123 tri-block copolymer solutions at different concentrations (10^{-6} -10^{-2} M) were conducted to study the forms of P-123 molecules in water and SBF. The critical micelle concentration and the changes in critical micelle concentration where the miceller structures start to form, were determined. Then all these chareterization studies were repeated with the hydrophobic drug loaded micelles. Two types of drug loading method were used in this studies and the following specific conclusions were obtained.

1) The surface tension behavior of P-123 was found to be divided into three concentration regions marked as Regions I, II and III. Region I is believed to consist principally of monomers whereas Region III involves fully developed micelles. The surface tension values were lower in SBF in Region I and same in Region II and III. However, the concentrations where dimmers-trimers and micelles form are lower in SBF.
2) There were differences among the characterization methods such as DLS, AFM, STEM, and TEM.
3) According to DLS results, the average size of P-123 micelles does not change much in the presence of BSA in DW or SBF.
4) According to AFM results, the average size of P-123 micelles were larger in the presence of BSA. This might be due to the preparation method of micelles that have been dried on substrates.
5) STEM and TEM results, on the other hand, were the images of actual situation of micelles. The sizes of P-123 micelles do not change but they easily form aggregates in the presence of BSA in the system.

6) The charge distribution of P-123 micelles became broader in the presence of BSA and narrow in the case of SBF.
7) According to DLS results, the presence of drug in micelles does not change the size of micelles in both water and SBF much. But STEM results show some increase in their sizes. The drug loaded micelles seem to aggregate in water and SBF but get dispersed in SBF in the presence of BSA.

REFERENCES

Adamson (1997). Kruss Tensiometer Users Manual. KRÜSS, Hamburg Germany.

Anderson, P., Ivanov, P., Emara, M. M., Villen, J., Gygi, S. P., (2011). Angiogenin-Induced tRNA Fragments Inhibit Translation Initiation. Molecular Cell 43;4, 613–623.

Ando, T., Uchihashi, T., Kodera, N., Miyagi, A., Nakakita, R., Yamashita, H., and Sakashita, M., (2006). High-Speed Atomic Force Microscopy for Studying the Dynamic Behavior of Protein Molecules at Work. Japanese Journal of Applied Physics, 45;1, 3B.

Arruebo, M., Fernández-Pacheco, R., Ibarra, M. R., and Santamaría, J. (2007). Magnetic nanoparticles for drug delivery. Nanotoday, 2, 3.

Blanchard, C. R., (1996). Atomic Force Microscopy. Springer Journals 1, 5.

Carter, D. C., and Ho, J. X. (1994). Structure of Serum Albumin. Adv. Protein Chem. 45; 153-203.

Cappella, B., Dietler, G., (1999). Force-distance curves by atomic force microscopy. Surface Science Reports 34, 1-104.

Drelich, J., Fang, C., and White, C. (2002). Measurement of interfacial tension in fluid systems. Encyclopedia of Surface and Colloid Science, 3152-3166.

Ensign, L. M., Cone, R., and Hanes J. (2012). Oral drug delivery with polymeric nanoparticles: The gastrointestinal mucus barriers. Advanced Drug Delivery Reviews 64;6, 557–570.

Franks, F., (1993). Protein Biotechnology: Isolation, Characterization, and Stabilization, 3.

Gaucher, G., Dufresne, M. H., Sant, V. P., Kang, N., Maysinger, D., and Leroux, J. C. (2005). Block copolymer micelles: preparation, characterization and application in drug delivery. J Control Release 09(1-3):169-88.

Guo, J., Ping, Q., Jiang, G., Huang, L., and Tong, Y., (2003). Chitosan-coated liposomes: characterization and interaction with leuprolide. International Journal of Pharmaceutics 260;2, 167–173.

Hunter, G. L., and Weeks, E. R. (2012). The physics of the colloidal glass transition. Rep. Prog. Phys. 75, 066501 (30pp).

Jachimska, B., and Pajor, A. (2012). Physico-chemical characterization of bovine serum albumin in solution and as deposited on surfaces. Bioelectrochemistry, 87, 138–146.

Jones, M. C., and Leroux, J. C. (1999). Polymeric micelles – a new generation of colloidal drug carriers. European Journal of Pharmaceutics and Biopharmaceutics 48, 101-111.

Jong, W. H., and Borm, P. J. A. (2008). Drug delivery and nanoparticles: Applications and hazards. Int J Nanomedicine, 3(2): 133–149.

Kedar, U., Phutane, P., Shidhaye, S., Kadam, V. (2010). Advances in polymeric micelles for drug delivery and tumor targeting. Nanomedicine: Nanotechnology, Biology, and Medicine 6, 714–729.

Kiss, É., Dravetzky, K., Hill, K., Kutnyánszky, E., and Varga, A., (2008). Protein interaction with a Pluronic-modified poly(lactic acid) Langmuir monolayer. Journal of Colloid and Interface Science 325;2, 337–345.

Mesa, C. L., (2005). Polymer–surfactant and protein–surfactant interactions. Journal of Colloid and Interface Science 286;1, 148–157.

Micic, M., Chen, A., Leblanc, R. M., and Moy, V. T., (1999). Scanning electron microscopy studies of protein-functionalized atomic force microscopy cantilever tips. 21;6, 394–397.

Mishra, B., Patel, B. B., Tiwari, S., (2010). Colloidal nanocarriers: a review on formulation technology, types and applications toward targeted drug delivery. Nanomedicine: Nanotechnology, Biology and Medicine, 6:1, 9–24.

Mourya, V. K., Inamdar, N., Nawale, R. B., and Kulthe, S. S. (2010). Polymeric Micelles: General Considerations and their Applications. Indian Journal of Pharmaceutical Education and Research.

Ochekpe1, N. A., Olorunfemi, P. O., and Ngwuluka, N. C. (2009). Nanotechnology and Drug Delivery Part 1: Background and Applications. Tropical Journal of Pharmaceutical Research, 8 (3): 265-274.

Ochekpe1, N. A., Olorunfemi, P. O., and Ngwuluka, N. C. (2009). Nanotechnology and Drug Delivery Part 2: Nanostructures for Drug Delivery. Journal of Pharmaceutical Research, 8 (3): 275-287.

Opanasopit, P., Yokoyama, M., Watanabe, M., Kawano, K., Maitani, Y., Okano, T., (2005). Influence of serum and albumins from different species on stability of camptothecin-loaded micelles. Journal of Controlled Release 104;2, 313–321.

Petrov, P., Yuan, J., Yoncheva, K., Müller, A. H. E., and Tsvetanov, C. B. Wormlike Morphology Formation and Stabilization of "Pluronic P123" Micelles by Solubilization of Pentaerythritol Tetraacrylate. J. Phys. Chem. B, 112 (30), 8879–8883.

Plapied, L., Duhem, N., Rieux, A., and Préat, V. (2011). Fate of polymeric nanocarriers for oral drug delivery. Colloid & Interface Science 16(3):228-237.

Rojas, O.J. (2002). ADSORPTION OF POLYELECTROLYTES ON MICA. Venezuela Encyclopedia of Surface and Colloid Science, 517.

Sachs, B. K., Thamboo, A., Lee, S. D., Wasan, K. M. (2007). Lipid excipients Peceol and Gelucire 44/14 decrease P-glycoprotein mediated efflux of rhodamine 123 partially due to modifying P-glycoprotein protein expression within Caco-2 cells. J Pharm Pharm Sci., 10(3):319-31.

Sahoo, S. K., and Labhasetwar, V., (2003). Nanotech approaches to drug delivery and imaging. Drug Discovery Today 8;24, 1112–1120.

Santos, S. F., Zanette, D., Fischer, H., and Itri, R., (2003)A systematic study of bovine serum albumin (BSA) and sodium dodecyl sulfate (SDS) interactions by surface tension and small angle X-ray scattering. Journal of Colloid and Interface Science, 262:2, 400–408.

Torchilin, V. P. (2007). Targeted pharmaceutical nanocarriers for cancer therapy and imaging. AAPS J., 9(2): E128–E147.

Tribout, M., Paredes, S., González-Mañas, J. M., Goñi, F. M., (1991). Binding of Triton X-100 to bovine serum albumin as studied by surface tension measurements. Journal of Biochemical and Biophysical Methods, 22:2, 129-133.

Valstar, A., Almgren, M., Brown, W., and Vasilescu, M., (2000). The Interaction of Bovine Serum Albumin with Surfactants Studied by Light Scattering. Langmuir, 16 (3), 922–927.

Wang, G., Nikolovska-Coleska, Z., Yang, C. Y., Wang, R., Tang, G., Guo, J., Shangary, S., Qiu, S., Gao, W., Yang, D., Meagher, J., Stuckey, J., Krajewski, K., Jiang, S., Roller, P. P., Ozel Abaan, H., Tomita, Y., and Wang, S., (2006). Structure- Based Design of Potent Small-Molecule Inhibitors of Anti-Apoptotic Bcl-2 Proteins. J. Med. Chem., 49 (21), 6139–6142.

Xu J., and Li, Y., (2006). Discovering disease-genes by topological features in human protein–protein interaction network. Oxford Journals 22;22, 2800-2805.

YANEVA, J., LEUBA, S. H., VAN HOLDE, K., and ZLATANOVA, J., (1997). The major chromatin protein histone H1 binds preferentially to cis-platinum-damaged DNA (anticancer drugsyDNA adductsyHMG1ylinker histones). Proc. Natl. Acad. Sci., 94, 13448–13451.

Yokoyama, M. (2005). Drug targeting with nano-sized carrier systems. Journal of Artificial Organs, 8, 77-84.

Yoncheva, K., Calleja, P., Agüeros, M., Petrov, P., Miladinova, I., Tsvetanov, C., and Irache, J. M., (2012). Stabilized micelles as delivery vehicles for paclitaxel. International Journal of Pharmaceutics 436;1–2, 258–264.